Distortion and Attenuation Free Gain-Assisted Superluminal Propagation in a Rare-Earth Doped Crystal

Antonius Johannes Renders
Supervisors: Lars Rippe, David Gustavsson and Adam Kinos

LUNDS UNIVERSITET

LTH Faculty of engineering
Division Atomic physics
Quantum Information group
Lund University
LRAP - 591
June 19^{th}, 2023

Abstract

A light pulse that travels through a narrow spectral window, i.e. a frequency range of low absorption, within a strongly absorbing frequency range will be delayed due to strong dispersion. If however, the absorbing structure is inverted, such that it is amplifying instead, one will see that a pulse travelling through this window will have its pulse peak come out of the material before it is sent in. This phenomenon is called superluminal propagation, light with negative group velocity or fast light. In this thesis negative group velocity of light through anomalous dispersion of a Europium-doped YSO crystal was studied. A spectral window of low absorption was created in the inhomogeneous profile. Within this spectral window, an absorbing structure is made up of two identical, equidistant from the centre frequency peaks ($\omega = \omega_0 \pm \omega_{\text{shift}}$). The structure was composed of ions with strong oscillator strengths, collected through reshuffling ions to different hyperfine levels. This allowed for the collection of a total absorption that exceeds the natural level near the centre frequency. Between the two absorption peaks a region of strong dispersion exists, the magnitude of the dispersion here is far higher in between the peaks than elsewhere in the created spectral window. This structure is then inverted to get a gain structure instead of an absorbing structure. This changes the sign of the dispersion and hence created a region of strong anomalous dispersion and allowed for the propagation of a Gaussian pulse with negative group velocity. This method is unique in that it does not alter the pulse shape or cause significant attenuation. Furthermore, this method allows for the isolated generation of a fast light pulse without the simultaneous generation of a slow light pulse. Through Maxwell-Bloch simulations and using estimates of the experimental conditions an optimal recipe was determined to create the maximal pulse advancement with respect to its time-bandwidth product. The simulations for the maximal width of the pit gave a frequency width of 29 MHz and the optimal width of the two gain structures was determined to be 1 MHz with a hole of 0.3 MHz in between them. The optimal αL from simulation was 12. However, due to experimental factors, an absorption of $\alpha L = 4.8$ had to be used. This allowed for a Gaussian propagation pulse with $t_{\text{FWHM}} = 5$ μs. Experimentally a group refractive index of $n_g \approx$-10135 was achieved and a pulse advancement of 10-14.2% of the t_{FHWM}, probe pulses had little to no distortion and little to no attenuation/amplification when remaining within the linear regime. A non linear relationship for the optimal αL - t_{FWHM} seems to exist.

Contents

α	Absorption coeff.	e	Electron charge
α_m	Material abs. coeff.	$\vec{E}$	Electric field vector
α_0	Host absorption coeff.	f_{12}	Oscillator strength
β	Wave vector	f_{lens}	Focal length lens
β_{kt}	Boltzmann factor	f_{scan}	freq. scan range
γ	Emission rate	g_1	Degeneracy level 1
γ_{rad}	Radiative decay rate	g_2	Degeneracy level 2
Γ_h	Homogeneous linewidth	h	Planck's const.
Γ_{in}	Inhomogeneous linewidth	$\hbar$	Reduced Planck's const.
ϵ_0	Vacuum dielectric const.	$\vec{H}$	Magnetic field vector in material
ϵ	Dielectric const.	I	Intensity
ϵ_r	Complex dielectric const.	I_0	Peak intensity
η	Optical impedance	$\vec{J}$	Current
$\theta_{1,2}$	Propagation angle	L	Crystal length
κ	Extinction coeff.	m	Mass
λ	Wavelength	m_e	Electron mass
λ_0	Vacuum wavelength	M	Magnification
μ	Permeability	M_r	Magnification in ray optics limit
$\vec{\mu}$	Dipole moment	n	Refractive index
μ_0	Vacuum permeability	N	Number density
μ_{21}	Dipole moment between levels 1 & 2	n_g	Group refractive index
ν	freq.	n_{host}	Host refractive index
ν_c	Central freq.	$\vec{P}$	Polarisation vector
ν_g	freq. width to the edge of gain structure	P	Power (laser)
ν_{pit}	freq. width hole	p_x	1D polarisation
ρ	Density matrix	$\vec{r}$	Position operator
σ	Conductivity	T	Temperature
$\tilde{\chi}$	Susceptibility	T_2	Dephasing time
ω	Angular freq.	t_{adv}	Pulse advancement
ω_0	Angular transition freq.	$t_{\text{cut-off}}$	Cut-off pulse duration
ω_{at}	Dopant angular transition freq.	t_{delay}	Time delay
Ω	Rabi freq.	t_{FWHM}	Time FWHM
A_{21}	Einstein coeff.	v_g	Group velocity
$\vec{B}$	Magnetic field vector	w_0	Beam waist radius
c	Speed of light	$w(z)$	Beam radius
c_0	Speed of light in vacuum	W_{12}	Transition rate
$c_{1,2}$	Population of lower, upper states	$Y_{1,2}$	Position beam input, output
$\vec{D}$	Displacement field	z_{R}	Rayleigh Length

1 Introduction

A light pulse propagates with something called the group velocity. The group velocity it describes the velocity at which the envelope of the amplitudes of the frequency components that make up the pulse travel. When the pulse travels in free space, it propagates at the speed of light. However when it travels in a material, the group velocity is effected by the refractive index and the change in refractive index with frequency, called dispersion, which usually reduces the group velocity as can be seen in equation 1.

$$v_g = \frac{c_0}{n + \nu_c \frac{dn}{d\nu}} \tag{1}$$

The dispersion, $\frac{dn}{d\nu}$, ordinarily varies only slightly with frequency and hence it tends to have a rather minor effect on the group velocity. In the proximity of resonances however, the dispersion can change rapidly. Looking back at equation 1, it is seen that the group velocity is reduced a lot when the dispersion becomes large. This is referred to as slow light. Slow light propagation occurs for normal dispersion, i.e. $\frac{dn}{d\nu} > 0$. If instead a material has a negative slope of the refractive index, i.e. anomalous dispersion, the group velocity will increase. And if it is strongly negative, the denominator in equation 1 can become smaller than one or even go negative. When this happens one speaks of "light with negative group velocity".
Negative group velocity of light, sometimes called superluminal light or fastlight is a fascinating physical phenomenon that was first theoretically described over a hundred years ago [1]. In the sixties, Sommerfeld and Brillouin further studied light in absorbing materials and theoretically showed that anomalous dispersion occurs inside an absorption line and that the group velocity that results is faster than the vacuum speed of light due to the wave nature of light [2]. Something physical being faster than the speed of light has subsequently been the subject of debate because it sounds as if causality would be violated. According to causality information transfer cannot exceed the speed of light in vacuum. So to find out if this occurs, let's look at what actually happens when a pulse is sent into a material with an anomalous dispersion region and get back to the causality question in a bit. Depicted in figure 1. A Gaussian pulse is impinging on a medium with strong anomalous dispersion, and before the pulse peak enters the material, it is reconstructed together with a counter-propagating 'anti-pulse' at the other end of the material. This anti-pulse cancels out incoming the pulse at the boundary. One sees that the pulse exiting the material is advanced compared to the input, so the pulse peak travelled faster than c_0. But did it transfer information? To answer this one has to look at the definition of information. Information is contained in discontinuities, and an analytical pulse, such as a Gaussian, is continuous in all space. Its wings extend into infinity and hence no new information is contained in the pulse peak. This means that shifting the pulse peak forward in space did not transfer any information. As a matter of fact, the pulse peak is merely reconstructed ahead in space by borrowing energy that was stored in the material and thus causality is not broken.

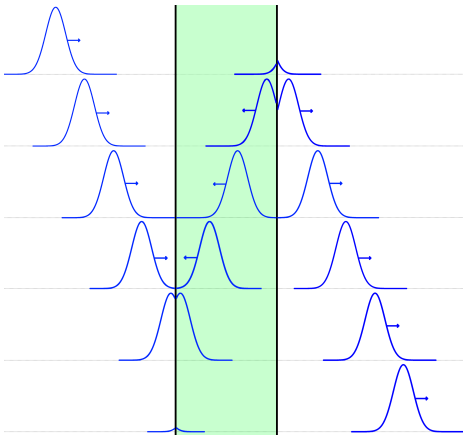

Figure 1: Visualisation of the fastlight effect when a pulse approaches a medium in the strongly anomalous regime (in green). Technically the pulse wings extend out into infinity, and hence the material "knows" the pulse shape ahead of time.

One of the first experimental confirmations, a 29 ps advancement was demonstrated in 1981 by Chu and Wong [3] albeit with a method that could not detect the pulse shape. This pulse was later reconstructed in simulation by Segard and Macke [4] who claim this pulse must have been heavily distorted. One might wonder what fastlight could be used for if no information transfer can be sped up. A few applications have been suggested, for example, that fastlight could be used for increased sensitivity for gravitational wave detection or for the realisation of white light cavities [5]. But for now, it remains to be seen if it will find an application in the near future.
Fastlight can be achieved in different ways. One approach is to create a narrow spectral hole in the absorption profile. A narrow hole generates a strong normal dispersion region around the hole centre frequency ω_0. This yields the slow light effect where the group velocity of the pulse is much lower than c_0, for a pulse with a frequency content that fits in this transparent range. Right outside the centre frequency of the spectral hole, there are two regions of anomalous dispersion. In other words, a region where the slope of the refractive index $\frac{dn}{d\nu}$ is negative. If one now creates two identical spectral holes equidistant in frequency, of some centre frequency, i.e. at $\omega_0 \pm \omega_{shift}$, there will exist a region of strong anomalous dispersion at ω_0. This has the drawback that the pulse has to be sent through a region of strong absorption which strongly attenuates the pulse, though the duration is maintained [6]. This approach was used by Segard and Macke [4] who used a 24 m long gas cell made out of a couple of circular waveguides, achieving an advancement of 2 μs on a $t_{\mathrm{FWHM}} = 8$ μs and significant pulse attenuation of 46 dB. Later Rajan et al. [6] carried out an experiment in emerald. They used the anomalous region in between two spectral holes in the inhomogeneous profile. With this configuration, an advancement of 25 ns was achieved on a pulse of 115 ns. Pulses again did suffer from strong

attenuation and were distorted.
An approach that didn't suffer strong attenuation was tested in 1966 in Soviet Russia, where it was shown that during nonlinear amplification the pulse peak can exceed c. They used a pulse with sufficient energy in the pulse front to completely de-excite the gain medium it travelled through. This caused the pulse front to take on the full energy of the medium while the tail of the pulse experienced attenuation through the now absorbing medium. Giving the pulse maximum additional forward momentum [7]. The resulting pulse is heavily distorted however with a long trailing tail and experiences a lot of amplification. Several other methods have been shown and further approaches include: fastlight inside a tunnelling barrier [8] and using an active plasma [9]. The same drawbacks are present in all these approaches, the pulse either suffers strong absorption or significant pulse reshaping.
Then it was shown [10] that one can create a region of anomalous dispersion in a transparent medium on the side of an absorption line. This would still affect the pulse shape but a little later it was proposed that one could use a gain doublet to create a lossless anomalous dispersion region which would not distort the pulse shape [11]. Dogariu et al. [2], [12] used a dilute atomic caesium vapour cell and pumped with two Raman pump fields to create two Raman gain lines in a Λ system. This leads to the transparent region with anomalous dispersion which they used to advance a Gaussian pulse with a $t_{\mathrm{FWHM}} \approx 3$ μs by 63 ns over a 6 cm cell. They reported a 40 % transmittance due to broadband absorption.
The Quantum information group in Lund has been working with rare-earth-doped-crystal (RE-crystal) for quantum computing for quite some time and has very good control over their materials. They have also worked on using slow light for laser stabilisation. Their RE-crystal was used for this project and has exactly the properties that make it an excellent candidate for achieving fastlight; it has a wide inhomogeneous absorption profile that far exceeds the homogeneous line width at cryogenic temperatures and a hyperfine lifetime that is more than weeks. This allows for the burning of extremely narrow spectral holes and hence the creation of a very steep refractive index slope. It also allows for the creation of a wide spectral pit creating a situation where one can create a gain structure that is isolated from any other absorbing parts, such that the refractive index slope $\frac{dn}{d\nu}$ caused by the ions far from the centre of the spectral pit, which would cause a slowlight effect, is negligible compared to that originating from the gain structure so the competing slow light effect is much smaller. Furthermore, the crystal has the strong inhomogeneous absorption profile along one polarisation axis and zero along the other.

2 Theory

This section treats the physics behind the fast light, an analytical description is derived and by the end of this section the reader will understand how to obtain fastlight experimentally. Like we saw in the introduction, the group velocity depends on the refractive index and its slope as a function of frequency. In this section we will see that the slope of the refractive index is strongly altered near resonances. If we look at a wide spectral pit of some tens of MHz in a broad absorbing region, depicted in figure 2 A, for example, and plot the resulting refractive index in the same figure, one can see there is only a relatively small effect at its centre frequency, but a rather strong change near the pit edges.
By tailoring the absorption profile, i.e. creating a narrow region of no absorption, often called a spectral hole or window, in between two regions of very strong absorption, the slope of the refractive index becomes very large, see figure 2 B, leading to slowlight and one can even stop light in a medium. The edges of the spectral features in respect to each other determine the slope, hence the narrower the spectral window and the wider and higher the features on the sides, the steeper the slope and stronger the effect.

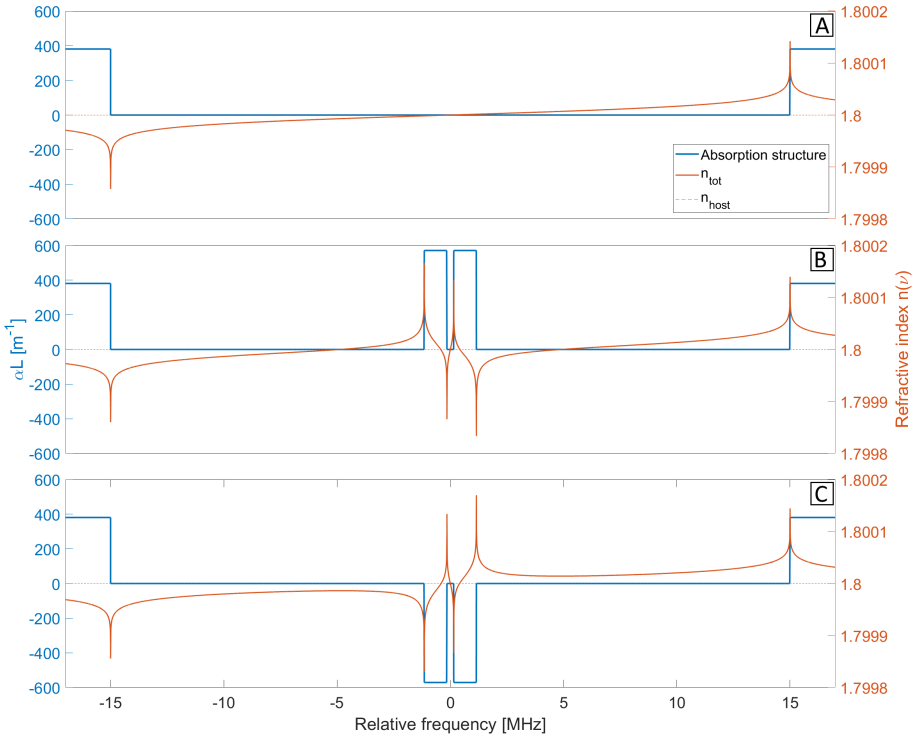

Figure 2: Simulation of the effect the spectral structure has on refractive index

In the usual scenario of an absorbing profile, this means a very large positive slope and hence the group velocity goes down. However, if we were to flip the sign, i.e. create a gain structure instead, then the slope will be flipped and the refractive index slope can become negative see figure 2 C, giving a group velocity that is larger than c_0, the speed of light in vacuum! If one takes equation 1 and makes the assumption $n \ll \nu_c \frac{dn}{d\nu}$ i.e. the strong dispersion regime, one can find the expression of how the group velocity depends on the absorption or gain structure:

$$v_g = \frac{1}{\alpha} \frac{\pi^2}{\frac{1}{\nu_{\text{hole}}} - \frac{1}{2\nu_g}} \tag{2}$$

Where α is the absorption coefficient, ν_{hole} the frequency width of the hole, and ν_g the frequency width from the centre of the hole up to the edge of the gain structure. See figure 3

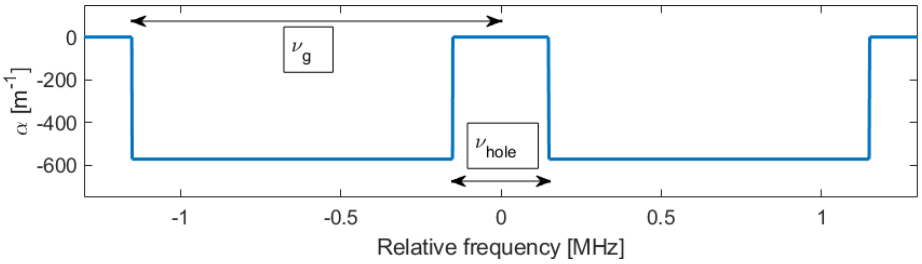

Figure 3: Figure to clarify what is meant by ν_g and ν_{hole}

We will now derive equation 2. To lay the groundwork for understanding the phenomena that will later be studied in simulations and experiment; the physics of negative group velocity is explored here. As the subject is light interaction with and propagation through a medium it is only natural to start with Maxwell's famous equations for electromagnetism in a medium:

$$\begin{aligned} \vec{\nabla} \cdot \vec{D} &= \rho \\ \vec{\nabla} \times \vec{E} &= -\frac{1}{c} \frac{\partial \vec{B}}{\partial t} \\ \vec{\nabla} \cdot \vec{B} &= 0 \\ \vec{\nabla} \times \vec{H} &= \vec{J} + \frac{\partial \vec{D}}{\partial t} \end{aligned} \tag{3}$$

With: $\vec{D} = \epsilon \vec{E} + \vec{P}$ the displacement field, ρ the charge density, $\vec{H} = \mu \vec{B}$ the magnetising field and $\vec{J} = \sigma \vec{E}$ the current and σ the conductivity. The particular medium that is part of the investigation can be described as a host medium and a collection of dopant atoms that are contained within said host, are the ones we interact with. Therefore in the remainder of the text when the

physics is a result of the host atoms that quantity "X" will be denoted with X_{host} and when it is due to the atoms X_{at}. Said atoms can be considered a collection of oscillators that respond to an external field with a polarisation, this response field is found using linear response theory. The response to a field with the form:

$$E_x(t) = \frac{1}{2}\left[\tilde{E}_x e^{j\omega t} + \tilde{E}_x^* e^{-j\omega t}\right] \tag{4}$$

where $\tilde{E}$ is the phasor of the electric field and ω the frequency, results in the polarisation response of the material:

$$p_x(t) = \frac{1}{2}\left[\tilde{P}_x e^{j\omega t} + \tilde{P}_x^* e^{-j\omega t}\right] \tag{5}$$

These two functions are then plugged into the classical model for an oscillator:

$$\frac{d^2 p_x(t)}{dt^2} + \left(\gamma + \frac{2}{T_2}\right)\frac{dp_x(t)}{dt} = \omega_{\text{at}}^2 p_x(t) = \frac{Ne^2}{m} E_x(t) \tag{6}$$

Here γ is the decay rate, T_2 the dephasing time which we'll briefly revisit later, when we talk about the actual experiment. Solving this gives:

$$\frac{\tilde{P}_x}{\tilde{E}_x} = \frac{Ne^2}{m}\frac{1}{\omega_{\text{at}}^2 - \omega^2 + j\omega(\gamma + \frac{2}{T_2})} \tag{7}$$

This is the expression for the susceptibility. When the medium in question is isotropic and linear there is also a direct relation between the polarisation and the electric field:

$$\tilde{P}(\omega) = \tilde{\chi}(\omega)\epsilon\tilde{E}(\omega) \tag{8}$$

Then when considering the response of the host material and the dopant ions separately the displacement can be rewritten as

$$\begin{aligned} \tilde{D} &= \epsilon_0\tilde{E} + \tilde{P}_{\text{host}} + \tilde{P}_{\text{at}} \\ \tilde{P}_{\text{host}} &= \tilde{\chi}_{\text{host}}\epsilon_0\tilde{E} \\ \epsilon_{\text{host}} &= \epsilon_0(1 + \tilde{\chi}_{\text{host}}) \\ \rightarrow \tilde{D} &= \epsilon_0[1 + \tilde{\chi}_{\text{host}}]\tilde{E} + \tilde{P}_{\text{at}} \\ \tilde{P}_{\text{at}} &= \tilde{\chi}_{\text{at}}\tilde{E} \end{aligned} \tag{9}$$

Where the last line gives the susceptibility that is most interesting for the fast light effect. The susceptibility observed at frequency ω can be expressed similarly to before as:

$$\tilde{\chi}_{\text{at}}(\omega) = \frac{\tilde{P}_x}{\epsilon\tilde{E}_x} = \frac{Ne^2}{m\epsilon}\frac{1}{\omega_{\text{at}}^2 - \omega^2 + j\omega\Delta\omega_{\text{at}}} \tag{10}$$

with $\Delta\omega_{\text{at}} = \gamma + \frac{2}{T_2}$ which is the atomic linewidth. Usually, the interesting physics occurs within a few linewidths from the transition. Hence, one can

make the resonance approximation $\omega \simeq \omega_{\text{at}}$ and $\omega^2 - \omega_{\text{at}}^2 \approx 2\omega_{\text{at}}(\omega - \omega_{\text{at}})$ which gives a simpler form of $\tilde{\chi}_{\text{at}}$ to work with:

$$\tilde{\chi}_{\text{at}}(\omega) = \frac{-jNe^2}{m\omega_{\text{at}}\epsilon(\Delta\omega_{\text{at}} + 2j(\omega - \omega_{\text{at}}))} \tag{11}$$

It is now time to move from a classical model to a real system that is quantum mechanically correct. We start with the definition of a classical oscillator radiative decay:

$$\gamma_{\text{rad}} = \frac{e^2\omega_{\text{at}}^2}{6\pi\epsilon mc^3} \tag{12}$$

then combine it with the classical oscillator susceptibility, substitute in the population difference density ΔN between the two levels of the transition and the result is the quantum susceptibility:

$$\chi_{\text{at}}(\omega) = -j\frac{3}{4\pi}\frac{\Delta N\lambda_0^3\gamma_{\text{rad}}}{n_{\text{host}}^3}\frac{1}{\Delta\omega_{\text{at}} + 2j(\omega - \omega_{\text{at}})} \tag{13}$$

here $\frac{\Delta N\lambda_0^3}{n_{\text{host}}^3}$ is the population difference contained in the volume of one cubic wavelength, $n_{\text{host}} = \sqrt{\mu\epsilon/\mu_0\epsilon_0} \approx \sqrt{\epsilon/\epsilon_0}$ if $\mu \approx \mu_0$. Now the interesting part starts! This susceptibility is namely the separate susceptibility that deals with the resonant oscillator part or atomic part of the laser medium and is related to the refractive index and this we want to manipulate. So lets get to that relation:

$$\eta = n + j\kappa = \sqrt{\epsilon_r} \tag{14}$$

where κ is the extinction coefficient, which is related to the susceptibility through:

$$\eta = \sqrt{1 + \chi} \tag{15}$$

The susceptibility is a complex quantity as one can see in equation 7 and it can thus be separated in real and imaginary parts:

$$\chi = \chi_{\text{real}} + j\chi_{\text{imag}} \tag{16}$$

so we get:

$$n + j\kappa = \sqrt{1 + \chi_{\text{real}} + j\chi_{\text{imag}}} \tag{17}$$

where $\kappa = \sqrt{\frac{1}{2}\left(\sqrt{\epsilon_{\text{real}}^2 + \epsilon_{\text{imag}}^2} - \epsilon_{\text{real}}\right)}$ If we are then in the weak susceptibility regime, i.e. $|\chi_{\text{real}}|, |\chi_{\text{imag}}| \ll 1$ then:

$$n + j\kappa \approx 1 + \frac{\chi_{\text{real}}}{2} + j\frac{\chi_{\text{imag}}}{2} \tag{18}$$

so there one can separate real part, linked to the refractive index and the imaginary part related to the absorption.

$$\begin{aligned} n &\approx 1 + \frac{\chi_{\text{real}}}{2} \\ \kappa &= \frac{\chi_{\text{imag}}}{2} \end{aligned} \tag{19}$$

There are two components in this absorption, one is associated with the atomic gain or loss, (depending on the sign), negative being absorbing due to the transition:

$$\alpha_m(\omega) = \frac{\beta}{2}\chi_{\text{imag}}(\omega) \tag{20}$$

where the propagation constant β was introduced, $\beta = \frac{2\pi n}{\lambda_0}$, and then there is the part due to the background absorption given by:

$$\alpha_0 = \frac{\beta}{2}\frac{\sigma}{\omega\epsilon} \tag{21}$$

where α is the absorption coefficient. It would be nice to now get to an expression that is describing a spectral pit, which is what we'll be working with. To give a peak at some of the future parameters and to justify some assumptions that will be made. In the experiment, the inhomogeneous linewidth of the atoms targeted will be 22 GHz and the spectral pit that will be created will be on the order of tens of MHz. Hence $\nu_{\text{hole}} \ll \Gamma_{inhomo}$, this will further down the line allow us to make the assumption that the inhomogeneous profile has a constant absorption coefficient. To simplify the notation a bit we replace the angular frequency with the frequency and now denote the linewidth by Γ_h and rewrite the population difference in terms of the absorption coefficient and considering a pit of width ν_{hole} centred at a frequency ν_c the susceptibility is written as:

$$\chi_h = -\frac{j\alpha_0 c}{\pi^2\nu_c}\frac{2n_{\text{host}}}{(2j\,(\nu-\nu_{\text{at}})+\Gamma_h)} \tag{22}$$

Since the real part is the most interesting for the fast light effect we just look at that, first multiplying both numerator and denominator of equation 22 by $(-2j(\nu-\nu_{\text{at}})+\Gamma_h)$ and then taking the real part gives:

$$\chi_{h,\text{real}} = \frac{4\alpha_0 c n_{\text{host}}}{\pi^2\nu_c}\frac{(\nu_{\text{at}}-\nu)}{\left(4\,(\nu-\nu_{\text{at}})^2+\Gamma_h^2\right)} \tag{23}$$

Now consider the lineshape function $g(\nu)$ of some inhomogeneous profile, this is a normalised quantity:

$$\int_{-\infty}^{\infty} g(\nu)d\nu = 1 \tag{24}$$

now one would like to compute:

$$\chi_{\text{real}} = \int_{-\infty}^{\infty} g(\nu)\chi_{h,\text{real}}(\nu)d\nu \tag{25}$$

This is not an easy task, but here the assumption made earlier comes to the rescue, namely that the real part of the susceptibility of an infinitely wide distribution with constant height is zero, so instead we can compute χ_{real} for just the pit with the gain structure and the background medium separately. First

to compute the real susceptibility for a wide pit one must evaluate the integral as:

$$\chi_{\text{real}_{\text{pit}}} = \int_{-\nu_{\text{pit}}/2}^{\nu_{\text{pit}}/2} \chi_{h,\text{real}} d\nu \tag{26}$$

which gives:

$$\chi_{\text{real}_{\text{pit}}} = \frac{\alpha_0 c n_{\text{host}}}{2\pi^2 \nu_c} ln\left(\frac{4\nu^2 + 4\nu_{pit}\nu + \Gamma_h^2 + \nu_{\text{pit}}^2}{4\nu^2 - 4\nu_{\text{pit}}\nu + \Gamma_h^2 + \nu_{\text{pit}}^2}\right) \tag{27}$$

which can be further simplified by realising that $\Gamma_h \ll \nu_{\text{pit}}$ giving:

$$\chi_{\text{real}_{\text{pit}}} = \frac{\alpha_0 c n_{\text{host}}}{\pi^2 \nu_c} ln\left(\frac{2\nu + \nu_{\text{pit}}}{2\nu - \nu_{\text{pit}}}\right) \tag{28}$$

The effect this has on the susceptibility is seen in figure 2 A.
Then for the structure in the pit, since the absorption in the pit is zero everywhere except for the parts where the structure is created, the lineshape can be approximated by step functions at these points and zero elsewhere, then the integral is split in two giving:

$$\chi_{\text{real}} = \int_{-\nu_g}^{-\nu_{\text{hole}}/2} \chi_{h,\text{real}} d\nu + \int_{\nu_{\text{hole}}/2}^{\nu_g} \chi_{h,\text{real}} d\nu \tag{29}$$

Given these limits, the integral can be solved, which gives:

$$\chi_{\text{real}} = \frac{\alpha_{\text{struct}} c n_{\text{host}}}{2\pi^2 \nu_c} ln\left(\frac{(4\nu^2 + 4\nu_{\text{hole}}\nu + \Gamma_h^2 + \nu_{\text{hole}}^2)(4\nu_g^2 - 8\nu_g\nu + 4\nu^2 + \Gamma_h^2)}{(4\nu^2 - 4\nu_{\text{hole}}\nu + \Gamma_h^2 + \nu_{\text{hole}}^2)(4\nu_g^2 + 8\nu_g\nu + 4\nu^2 + \Gamma_h^2)}\right) \tag{30}$$

This would give the aforementioned absorbing structure, and when combined with the pit χ_{real}:

$$\chi_{\text{real}} = \frac{\alpha_{\text{struct}} c n_{\text{host}}}{2\pi^2 \nu_c} ln\left(\frac{(4\nu^2 + 4\nu_{\text{hole}}\nu + \Gamma_h^2 + \nu_{\text{hole}}^2)(4\nu_g^2 - 8\nu_g\nu + 4\nu^2 + \Gamma_h^2)}{(4\nu^2 - 4\nu_{\text{hole}}\nu + \Gamma_h^2 + \nu_{\text{hole}}^2)(4\nu_g^2 + 8\nu_g\nu + 4\nu^2 + \Gamma_h^2)}\right) + \frac{\alpha_0 c n_{\text{host}}}{\pi^2 \nu_c} ln\left(\frac{2\nu + \nu_{\text{pit}}}{2\nu - \nu_{\text{pit}}}\right) \tag{31}$$

one gets figure 2 B. When the structure is then inverted, the sign of α_{struct} switches and one obtains figure 2 C. Now that there is an expression for χ_{real} the refractive index can be written down for the host and pit:

$$n = n_{\text{host}} + \frac{\chi_{\text{real}}}{2n_{\text{host}}} \tag{32}$$

to visualise the result, it is plotted in figure 2 overlaid with the three aforementioned structures, the values used for this calculation are the actual ones that came forth from the simulations for the optimal situation.

Again the region of interest is right in the middle of the pit, and here one can assume that the change in refractive index is linear to first order and with Taylor expansion of equation 32 and then using that $\Gamma_h \ll \nu_{\text{hole}}$ one gets:

$$n = n_{\text{host}} + \frac{\alpha_0 c}{2\pi^2 \nu_c}\left(\frac{2}{\nu_g} - \frac{4}{\nu_{\text{hole}}}\right)\nu \tag{33}$$

Finally, one can then plug this into the expression for the group velocity 1 and get equation 2. This means that if one would now send a pulse with a spectral bandwidth within the ν_{hole} it would gain the group velocity from equation 2

2.1 Coherent excitation and the collection of αL

The goal is naturally to create the largest fast light effect possible and to do that one must create a structure with the strongest possible gain structures and the narrowest hole that will fit the propagation pulse. To get the peaks one could simply burn a narrow hole on the top of the inhomogeneous line and then try to invert the population to get gain. But it is possible to do better. For starters Eu:YSO has two electronic states with three hyperfine splittings for both the excited and the ground state, see figure 4. In general, a two-level system means that one cannot simply blast the crystal with as much power as available and achieve complete population inversion. From the rate equations, one can see that two-level systems in steady-state do not allow complete population inversion. Therefore one must be more clever and instead coherently excite the ions. This does impose some limitations, the excitation must be done in one go, the excitation time is limited by the decay time and the decoherence time and finally, not all hyperfine transitions are equally strong and hence depending on the optical power available one might not be able to fully invert the population of some transitions. This is the reason that in figure 2 C the gain structure is surrounded by a wide pit without absorption, the power available would simply not suffice to excite extremely wide structures. To describe the coherent excitation of a two-level system, consider the following: a two-level system interacting with a monochromatic field of the form: $e\vec{r} \cdot \vec{E_0} cos(\omega t)$, then the relation of the populations c_1, c_2 of the ground and excited states respectively are related through:

$$i\frac{dc_1}{dt} = c_2\left(e^{i(\omega-\omega_0)t} + e^{i(\omega+\omega_0)t}\right)\frac{\Omega}{2} \tag{34}$$

where Ω is the Rabi frequency [13] and then using the rotating wave equation and solving for the initial condition that the entire population starts in the ground state, at resonance with the transition i.e. $\omega = \omega_0$ the population of the excited state is given as:

$$|c_2(t)|^2 = \sin^2\left(\frac{\Omega t}{2}\right) \tag{35}$$

That shows that if $\Omega t = \pi$ the population in the excited state is 1, so population inversion is achieved. This is a so called π-pulse. There exists a pulse called a sechyp that is commonly used to transfer the population of a narrow frequency

range to the excited state. However in the experimental part of this thesis, one would like to coherently excite a range of a few MHz wide and this can be done with a so-called sech-scan pulse, which is in a sechyp pulse split in two with a scan over a frequency range in between. Sechyp is short for complex hyperbolic secant pulse and is defined as:

$$\Omega(t) = \Omega_0 \text{sech}(\beta t)^{1+j\mu} \tag{36}$$

where Ω_0 is the centre Rabi frequency, β and μ are real. The sechyp pulse can transfer the population without any inhomogeneous dephasing, it allows for narrow excitation ranges as the transfer efficiency outside of the chirp window is very low, and it is very robust against fluctuations in the Rabi frequency. [14]

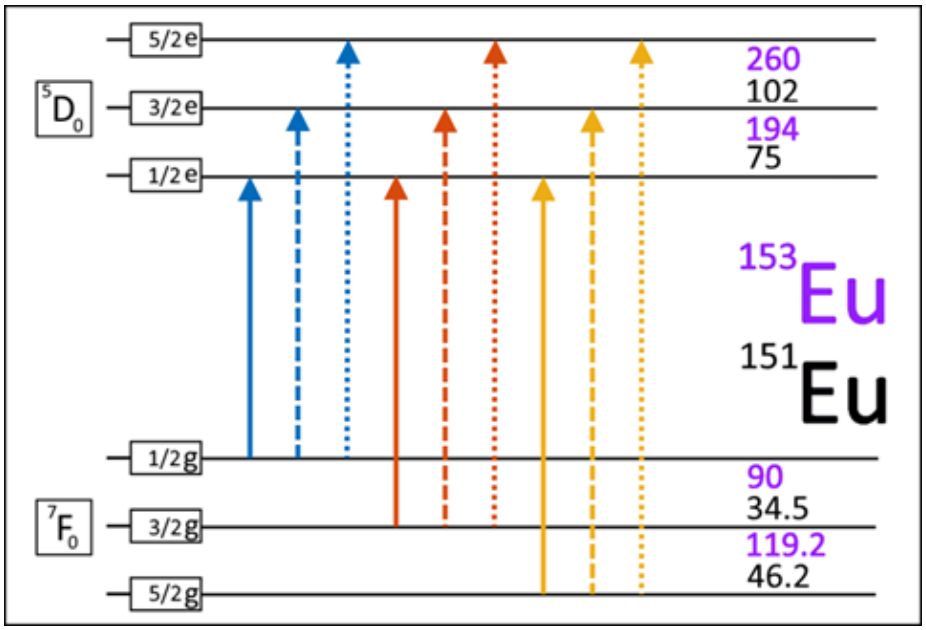

Figure 4: Schematic representation of the hyperfine levels in Eu:YSO with the splittings in MHz for both the isotopes

The hyperfine levels of Eu:YSO are depicted in figure 4. There are nine possible transitions for each isotope and these can be used to shuffle ions around and create the structure out of only the ions with high relative oscillator strength, theses are shown in table 2. This shuffling around can be understood as follows. Consider the inhomogeneous profile when it is undisturbed. In this state, the three ground states are equally populated. One can then excite an electron from for example the $|1/2g\rangle$ state to one of the excited states and then let it de-excite to one of the ground states. If it falls down where it started it will absorb again at the same frequency, however, if it falls down to the $|3/2g\rangle$ state

it will absorb at a frequency that is shifted by the hyperfine spacing of the two ground-states. Doing this repeatedly allows for the collection of ions at a desired frequency. Naturally this also applies to the excitation, an ion absorbing at a frequency 0 MHz relative to the inhomogeneous line from, $|1/2g\rangle \rightarrow |1/2e\rangle$ will also absorb to $|3/2e\rangle$ 75 MHz from the centre of the line. Making use of the fact that ions absorb at several frequencies one can then target an individual class that absorbs at a shared frequency with different classes. For example; if ion A absorbs at frequencies -2, 0 and 2 and Ion B absorbs at frequencies -3, 0, 3 and we would want to remove only ion A from frequency 0, we could excite it at frequency -2 or 2 instead to not disturb ion B. This is how undesirable ions could be removed from the created structure once it is created.

2.1.1 Rabi frequency, oscillator strength and laser intensity

To find out how much Rabi frequency is available to do the inversion one starts simply at the intensity of the laser which is related to the electric field through:

$$I = \frac{1}{2} nc\epsilon_0 |E|^2 \tag{37}$$

this is related to the Rabi frequency through:

$$\Omega = \frac{\mu E}{h} \tag{38}$$

or if one wants to have it expressed in the intensity instead:

$$\Omega = \frac{\mu \left| \sqrt{2I(r,z)/nc\epsilon_0} \right|}{h} \tag{39}$$

so here one must find an expression for the dipole moment μ which is done through the Einstein coefficient A_{21}. Assuming non-degenerate states and denoting the upper and lower state by 2 and 1 respectively:

$$A_{21} = \frac{2e^2\omega_{21}^3}{3\epsilon_0 hc^3} |\langle 1| \vec{r} |2\rangle|^2 \tag{40}$$

then for absorption the transition dipole moment is given as:

$$e^2 |\langle 1| \vec{r} |2\rangle|^2 = \mu_{21}^2 \tag{41}$$

which when combined gives:

$$\mu_{21}^2 = A_{21} \frac{3\epsilon_0 hc^3}{2\omega_{21}^3} \tag{42}$$

which is then related to the oscillator strength through:

$$f_{12} = \frac{g_2}{g_1} \frac{2\pi\epsilon_0 m_e c^3 A_{21}}{\omega_{21}^2 e^2} \tag{43}$$

where m_e is the mass of an electron, e the electron charge, ϵ_0 the vacuum dielectric constant, $g_{1,2}$ the degeneracies of the levels and h Planck's constant [15]

2.2 Amplified Spontaneous Emission

To maximise the fast light effect one must create the largest change in the slope of the refractive index. This means that one would like to collect as many ions in the excited state as possible. Practically however, the desired amount of collected ions and hence the gain is limited by a couple of factors. Since a two level system is being driven, to achieve full inversion the ions must be excited coherently, which means that the optical lifetime reduces the time power can be delivered to the crystal and is also affected by decoherence. Hence, the power that can be delivered by the excitation pulse is important. Another factor is amplified spontaneous emission (ASE) which reduces the optical lifetime in proportion to the amount of gain. Hence increasing the gain reduces the time available for the probe pulse. With a few assumptions, one can make a decent estimate of how much ASE is tolerable for this experiment. Starting with the assumption that the inverted region of the crystal is cylindrically shaped and has a diameter of $2r$ and length L rather than the Gaussian beam shape. Then a spectral packet emitted by a given volume of crystal is given by:

$$N\hbar\omega\gamma_{\text{rad}}$$

N being the density of inverted ions and γ_{rad} the radiative decay rate. A spectral packet originating from near the edges of the rod will give the largest contribution to the ASE and considering such a packet, the ASE is incremented in intensity by:

$$dI = \frac{\pi r^2 N\gamma_{\text{rad}}\hbar\omega}{4\pi L} e^{\alpha(L-z)} dz \tag{44}$$

Integrating this over the length of the rod and assuming that the total gain along the rod is very high yields the ASE intensity as:

$$I \approx \frac{\gamma_{\text{rad}}\hbar\omega r^2}{4\sigma L^2} e^{\alpha L} \tag{45}$$

This is simply stimulated emission from said initial wave packet for which the transition rate is given by [16] :

$$W_{12} = \frac{3}{8\pi^2} \frac{\epsilon |E|^2}{1 + [2(\omega - \omega_a/\Delta\omega_1)]^2} \tag{46}$$

which can be rewritten using eq 37 into:

$$W_{12} = \frac{\sigma I}{\hbar\omega} \tag{47}$$

hence:

$$\frac{W_{12}}{\gamma_{\text{rad}}} \approx \left(\frac{r}{2L}\right)^2 e^{\alpha L} \tag{48}$$

One can then rewrite the beam radius in terms of the Rayleigh length, (see equation 53), and find the αL given the other beam parameters which yields:

$$\frac{W_{12}}{\gamma_{\text{rad}}} \approx \left(\frac{\sqrt{\frac{z_R\lambda}{n\pi}}}{2L}\right)^2 e^{\alpha L} \rightarrow \alpha L = ln\left(\frac{W_{12}}{\gamma_{\text{rad}}} \frac{4L^2 n\pi}{z_R\lambda}\right) \tag{49}$$

Say that we are willing to accept a halving of the lifetime due to ASE, i.e. $W_{12} = \gamma_{\text{rad}}$ and that $z_R \approx L$ this gives the $\alpha_{max}L \approx 13$. The exact choice of this will depend on what the experimental constraints turn out to be however.

2.3 Beam through the crystal

A Gaussian beam will have its highest intensity at the centre of the beam and drop off like a Gaussian from there out radially, the intensity at a location z away from the beam waist w_0 and at radial distance from the beam axis is given by:

$$I(r,z) = I_0 \left(\frac{w_0}{w(z)}\right)^2 exp\left(\frac{-2r^2}{w(z)^2}\right) \tag{50}$$

where $r = \sqrt{x^2+y^2}$ and the peak intensity I_0 at the beam waist and axis is given by:

$$I_0 = \frac{2P}{\pi w_0^2} \tag{51}$$

Therefore one must make sure that the intensity at some radius r is still enough to invert the population. The beam width at any position along the direction of propagation z is given by:

$$w(z) = w_0 \left[\sqrt{1+\left(\frac{z}{z_R}\right)^2}\right] \tag{52}$$

Which is the radius that contains 86% of the beam power [17]. There will be a trade off between a collimated beam and its intensity that has to be made since intensity increases with decreasing area but collimation reduces. So the beam waist and focus in the crystal must be chosen in such a way that there will be enough intensity throughout the whole crystal and not just at the focal point. A good measure of this is the depth of focus Gaussian beam:

$$2z_R = \frac{2\pi w_0^2}{\lambda} = \frac{2\pi n w_0^2}{\lambda_0} \tag{53}$$

where z_R is known as the Rayleigh range [17]. It has been defined by the axial distance within which the beam is no greater than a factor $\sqrt{2}$ time its minimum value, i.e. at the beam waist, such that the area is at most factor 2 larger than at the beam waist. Since the crystal properties are known, using this equation the minimum beam size at the edge of the crystal can be determined by setting z at the edge of the crystal. Then one has to choose where one wants the focus. One choice would be to take w_0 in the middle of the crystal, see figure 5. Doing so and then taking the derivative of $w(z)$ towards w_0 and setting this to zero, plugging equation 53 into equation 52 yields:

$$\frac{\partial w(L/2)}{\partial w_0} = \frac{\partial}{\partial w_0}\left(w_0\left[\sqrt{1+\left(\frac{L\lambda}{2\pi w_0^2}\right)^2}\right]\right) = 0 \tag{54}$$

One could also argue that it would be best to have the focus at the far face of the crystal, since that is where the intensity is needed most and hence it could also make sense to put the beam waist there. This can also be calculated with equation 54 by simply replacing $L/2$ by L. The crystal that we have is $L = 21$ mm long, the optical wavelength of the Europium is $\lambda = 580$ nm and using this we find that the minimum is at $w_0 = 32.8$ μm when focused in the middle of the crystal and 46.4 μm when focused at the far face. Plugging this back into equation 52 gives a minimum beam-size of $w(L/2) = 46.4$ μm hence a beam diameter of 92.8 μm and $w(L) = 65.6$ μm so 131 μm diameter.

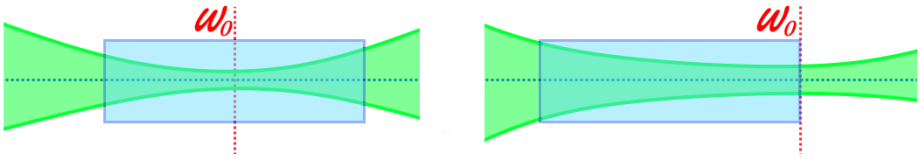

Figure 5: Two options for where to focus, either the centre of the crystal or the end of the crystal.

Now it is worth looking back quickly at the previous section about the ASE, the focus in the middle of the crystal has shorter Rayleigh length and tighter focus the crystal, (see figure 5), this reduces the number of paths that can contribute to the ASE somewhat, as compared to the end case since fewer spectral packets will reach the other side by traversing a region of strong gain / emission.
Since we start out with a beam that has a beam diameter of 1 mm , it must first be expanded so that it can then be focused down to the calculated minimum in the crystal using lenses. The setup is depicted in figure 6.

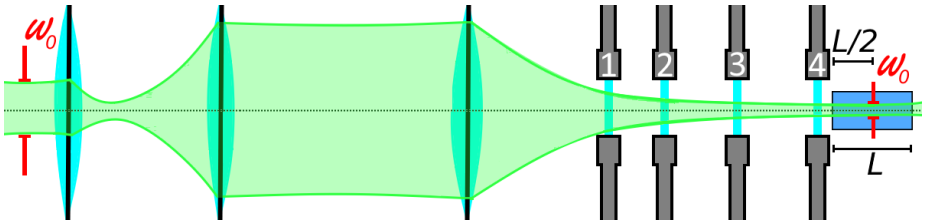

Figure 6: Schematic beam expander, focusing lens and cryostat windows marked with 1,2,3,4

The lenses were chosen due to the physical constraints of the system, namely a focus of $w_0'' = 32.8$ μm in the crystal which is ≥ 30 cm away from the lens, 25 cm due to the cryostat and ≈ 5 cm more to allow for for analysis of the beam quality with a beam-pick-off and fine tuning / adjustments of the focusing lens with a moving stage. The change of the focal point due to the four windows

refractive indices and crystal refractive index must also be taken into account. This can be done using matrix optics. In a ray-optics picture a ray travelling through an arbitrary optical system may be represented by:

$$\begin{bmatrix} y_2 \\ \theta_2 \end{bmatrix} = \begin{bmatrix} A & B \\ C & D \end{bmatrix} \begin{bmatrix} y_1 \\ \theta_1 \end{bmatrix} \tag{55}$$

There are essentially three different components in the focusing setup, a lens, free space and a number of parallel transparent plates (windows and crystal), giving the following transfer matrices:

$$\text{lens} = \begin{bmatrix} 1 & 0 \\ -\frac{1}{f_{\text{lens}}} & 1 \end{bmatrix} \quad \text{free space} = \begin{bmatrix} 1 & d \\ 0 & 1 \end{bmatrix} \quad \text{N parallel plates} = \begin{bmatrix} 1 & \sum_{i=1}^{N} \frac{d_i}{n_i} \\ 0 & 1 \end{bmatrix} \tag{56}$$

Where d, d_i are the various lengths through free space or material and n_i their respective refractive indices and f_{lens} the focal length of the lens. The Gaussian beam through a lens undergoes the following parameter transformations [17]:

$$\begin{aligned} w_0' &= M w_0 \\ (z_0' - f_{\text{lens}}) &= M^2 (z_0 - f_{\text{lens}}) \\ M &= \frac{M_r}{\sqrt{1 + r^2}} \\ r &= \frac{z_R}{z_0 - f_{\text{lens}}} \\ M_r &= \left| \frac{f_{\text{lens}}}{z - f_{\text{lens}}} \right| \end{aligned} \tag{57}$$

Where w_0' denotes the beam waist after the lens, z_0' the location of the beam waist after the lens with respect to the lens and z the same but before the lens. M is the magnification. The telescope is used to telescope the beam from 1 mm up to 4 mm and is then focused down into the crystal with a 400 mm lens. These calculations are then fed in to a tool called "Gaussian beam" to give the distances between the lenses such that the focus lies exactly in the middle of the crystal.

The expectation was that the laser power would be around $P \approx 30$ mW so $I_0 \approx 18$ MWm^{-2}. I_0 is the peak irradiance at the centre of the beam, at the beam waist [17].

This means that at the edge of our crystal. i.e. $L = 0.0105$ m the FWHM of the Gaussian is at radius:

$$ln\left(\frac{1}{2}\right) = \frac{-2r^2}{w(0.0105m)^2} \rightarrow r = 27.3\mu m \tag{58}$$

So at $r = 27.3$ μm and $z = \frac{L}{2}$ the intensity will be $I \approx 6.29$ MWm^{-2}. Using

equations 37, 39, 43 and 51, the constants and the f_{12} from table 3 gives:

$$\mu_{12} = \sqrt{f_{12}\frac{3}{4\pi}\frac{e^2 h}{m_e \omega_{12}}} = 6.8 \cdot 10^{-33} \text{ Cm}$$
$$\Omega = 6.8 \cdot 10^{-33} \frac{\left|\sqrt{2I(r,z)/nc\epsilon_0}\right|}{h} \tag{59}$$

$\Omega \approx 372$ kHz worth of Rabi frequency. Then there are three different transitions used with relative oscillator strengths of 0.85, 0.75 and 0.68 (see table 2) so taking the average of these three gives an average $\Omega \approx 283$ kHz

3 Crystal properties

In this thesis the experimental work was carried out on an $Eu^{3+}Y_2SiO_5$ in full Europium doped Yttrium orthosilicate (Eu:YSO) crystal. The dimensions of the crystal are 21 × 14 × 15 mm. It has a doping level of 1% and contains both the 151 and 153 isotopes in roughly equal proportions. This crystal has interesting properties for quantum information applications and can be used for slow light reference cavities for laser stabilisation [18]. The difference between the sites stems from the neighbouring atoms, it is either surrounded by 7 or by 6 oxygen atoms on site 1 and site two respectively. The Europium substitutes the Yttrium at those sites.

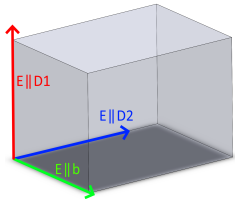

Figure 7: Scale version with crystal axis indicated

The isotopes also have different hyperfine spacings. In this thesis, all work is done at site 1 and both isotopes are considered. However the hyperfine spacing in isotope 153 is much larger than that in 151 and the acousto-optic-modulator (AOM), used to shift the light frequency, has a limited bandwidth, which limits the accessibility of the hyperfine levels in 153, since ions get shuffled further away in frequency than the range of this bandwidth they cannot be excited anymore and one cannot collect them. Site 1 is the interesting one for this project because of its absorption properties. Site 1 has a higher oscillator strength, $f = 3.4 \cdot 10^{-8}$ compared to $f = 1 \cdot 10^{-8}$ for site 2 [19]. The oscillator strength is transition dependent hence one can find different values in different publications [19, 20, 21], Könz et al. [21] use an average for example, hence the lower value. In

this work the strongest transitions are targeted, which for the $|3/2g\rangle \rightarrow |3/2\rangle$ transition was found by Lauritzen et al. [20] to be $f = 3.08 \pm 0.01 \times 10^{-8}$, where they note that it might be underestimated. This motivates the choice of the value reported by Thiel et al. which is noted in table 3. The absorption is given along three polarisation axis, $E \parallel D1$, $E \parallel D2$ and $E \parallel b$ that correspond to the physical crystal axis (not the axis of the unit cell of YSO). The absorption coefficient α_0 depends on the doping concentration this crystal has been doped at 1%. The crystal properties of importance are given in table 3:

Table 1: Table of important crystal properties at 2 K. [19][21]

Γ_{in}[GHz]	α_0[m^{-1}]			f	n_{host}	T_2[ms]	T_1[ms]
	E$\parallel$D1	E$\parallel$D2	E$\parallel$b				
22	390	80	$\approx$0	$3.4{\cdot}10^{-8}$	1.8	2.6	1.94

The inhomogeneous linewidth Γ_{in} at this site is 22 GHz FWHM ($\approx$ Lorentzian), $T_2 = 1/\pi\Gamma_h$ is the dephasing time [21]. Whereas site 2 has lower and roughly equal absorption along both $E \parallel D1$ and $E \parallel b$, which makes it less interesting for obtaining a large negative group velocity. The two sites are separated by some THz however so they are no competing factors.

4 Simulations

A computer simulation of a system with all six hyperfine levels is initiated and the population is assumed to be equally divided over the three ground states. This assumption can be made because the hyperfine energy splittings are in the tens of MHz for ^{151}Eu and around a hundred for ^{153}Eu when these values are plugged into the Boltzmann distribution equation, (in appendix 60), they will give equal probabilities even at temperatures around 2 K. [22] The reason that the structures can still persist as long as they do is that there are no phonons to re-thermalise the populations.

4.1 Pit burning

To create a spectral window, a pit is burned by frequency scanning over a range of 34 MHz around the centre frequency of the inhomogeneous profile. It is important that no ions that absorb at frequencies at the edges of the pit get dropped back into the pit. Since the crystal contains two isotopes one must take both ions into account when burning the pit. It turns out that if there was only the 153 isotope, the pit that can be burned is a lot larger, so the limiting factor is the 151 isotope. The two sites have transition frequencies that are so far apart that they will not interfere. The difference between the isotopes is also a big factor when burning back the ions. It is important that the pit is fully emptied. Any undesired absorption in the pit will deteriorate the fast

light. And one cannot just burn the structure straight into the inhomogeneous profile as this would leave behind ions that cannot be inverted since the Rabi frequency available would not be sufficient.

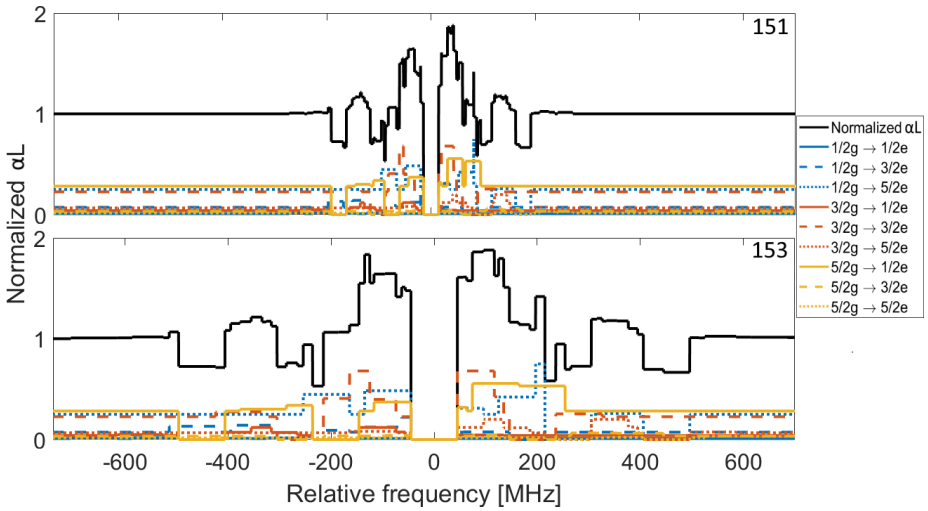

Figure 8: Maximum pit sizes for both isotopes

The pit burning simulation was done with a frequency sweep, broadening in this case is not important. To get a clean pit the pit had to be swept multiple times to get good results the sweep had to be done at least sixty times. In the experiment, it was done 100x to be safe.

4.2 Burning back the ions

To create the structure that is to be inverted ions must be burned back into the spectral window. This is done using the same principle as when the ions are burnt away, but now one carefully selects a frequency detuning. This specific detuning is determined by the hyperfine spacing, shown in figure 4 and the ion class one wants to collect. The oscillator strengths are used to determine the selection of the ions that one wants to collect. Higher oscillator strength means the probability for that transition is higher at a given Rabi frequency. The relative oscillator strengths of the transitions are given in table 2. The ions are sent back to the desired position by a series of sechscan pulses. One could use frequency scans to burn back the structure but using the sechscan excites a narrower frequency range.

	$\|1/2e\rangle$	$\|3/2e\rangle$	$\|5/2e\rangle$
$\|1/2g\rangle$	0.03	0.22	0.75
$\|3/2g\rangle$	0.12	0.68	0.20
$\|5/2g\rangle$	0.85	0.10	0.05

Table 2: Relative transition probabilities γ_{ij} for ^{153} EU^{3+}:Y_2SiO_5 taken from Laurtizen et al. [20] The uncertainty in each probability is estimated to be about $\pm$ 0.03. The transition probabilities are assumed to be the same for both isotopes.

Here it is seen that the cross terms, $|1/2g\rangle \rightarrow |5/2e\rangle$, $|3/2g\rangle \rightarrow |3/2e\rangle$, $|5/2g\rangle \rightarrow |1/2e\rangle$, are the strong oscillators and all three are close enough in Rabi frequency to each other that the can all be collected and excited thereafter.
These can be selected by looking at the level separation of transitions and burning accordingly. Here ten sets of frequencies were targeted. The resulting structure is shown in figure 9. This was simulated using software developed by Adam Kinos [23] that keeps track of all the inhomogeneously broadened ions and the probabilities of transitions to all separate hyperfine states and their different absorption frequencies before and after excitation.

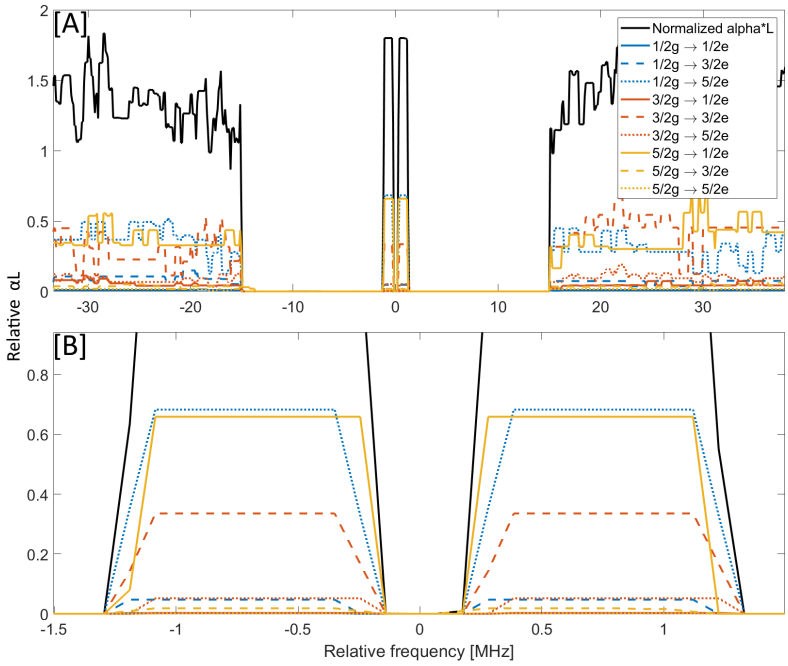

Figure 9: Structure created, full overview [A] and zoomed in on the gain structure [B]

Table 3: From where ions were collected and where they were collected to, together with the "burn back detuning" in MHz

Isotope	Wanted transition collected	Transition excited to burn back	Burn back frequency offset from pit centre
151	$\|1/2g\rangle \rightarrow \|5/2e\rangle$	$\|3/2g\rangle \rightarrow \|3/2e\rangle$	[-68.18;-66.68]
	$\|1/2g\rangle \rightarrow \|5/2e\rangle$	$\|5/2g\rangle \rightarrow \|3/2e\rangle$	[-21.92;-20.59]
	$\|3/2g\rangle \rightarrow \|3/2e\rangle$	$\|1/2g\rangle \rightarrow \|1/2e\rangle$	[-110.3;-108.8]
	$\|3/2g\rangle \rightarrow \|3/2e\rangle$	$\|5/2g\rangle \rightarrow \|3/2e\rangle$	[-29.52;-28.18]
	$\|5/2g\rangle \rightarrow \|1/2e\rangle$	$\|3/2g\rangle \rightarrow \|1/2e\rangle$	[-46.90;-45.45]
153	$\|1/2g\rangle \rightarrow \|5/2e\rangle$	$\|5/2g\rangle \rightarrow \|5/2e\rangle$	[-51.52;-50.07]
	$\|1/2g\rangle \rightarrow \|5/2e\rangle$	$\|3/2g\rangle \rightarrow \|5/2e\rangle$	[89.24;90.74]
	$\|3/2g\rangle \rightarrow \|3/2e\rangle$	$\|3/2g\rangle \rightarrow \|1/2e\rangle$	[-72.54;-71.04]
	$\|5/2g\rangle \rightarrow \|1/2e\rangle$	$\|3/2g\rangle \rightarrow \|1/2e\rangle$	[-119.2;-118.5]
	$\|5/2g\rangle \rightarrow \|1/2e\rangle$	$\|3/2g\rangle \rightarrow \|3/2e\rangle$	[71.08;72.58]

Some of the structure that has been burnt back comes with some unwanted transition that absorbs at the same frequency. This will deteriorate the gain, since there is not enough Rabi frequency to invert them, and counteracts the fast light effect, which is undesirable. To deal with this what can be done is either cleaning up transitions beforehand by burning in other places where that specific ion absorbs, or afterwards. This could have been employed had there been a crystal consisting entirely out of the 151 isotope, since for that one the transitions lie close enough such that by burning elsewhere the unwanted transitions can be removed. In 153 they are separated further in frequency to such an extent that it falls outside of the range of the AOM and thus it is not possible to clean up the structure.
Furthermore if one were to create the "perfect" structure in 151 the spacing in 153 is such that one cannot actually place the structure in that isotope in the way one would like. This would lower the possible αL dramatically down from $\approx$16.4 to $\approx$4.9. Therefore we have to accept that there will be some ions we cannot invert in our structure. As of now, it is estimated that this will effectively reduce the gain by twice the αL these unwanted transitions would have. Summed up in simulations the unwanted αL would thus be 1.1, which would correspond to a reduction of 2.2 in αL, in the worst-case scenario. Hence the maximum gain remaining would be a factor of $\approx$ 14.2.
During the burning back of the structure some unwanted ions are again collected in the pit. The unwanted ions in the pit that are far enough away in frequency from the structure can be burnt away again using a series of frequency scans. Those that are close to the structure are burnt away with sechscans instead. The ions that make up the burnt-back structure are subject to hyperfine broadening, resulting in the structure not having sharp edges and being spread out. To avoid this the structure is burnt back wider in frequency, 1.4 MHz wide instead of 1 MHz, and it is then made narrower with the aforementioned sechscans. The parameters of the sechscans are determined using Maxwell Bloch simulations. One such simulation result is shown in the appendix in figure 32, which was the

pulse designed for the cleaning up of the hole in the structure, because of the very narrow homogeneous linewidth this can be done to some kHz precision. Similar pulses are used for the outer edges of the structure. To avoid power broadening the power during the back-burning is limited and instead sixty iterations of the back-burn pulses are performed with a waiting time of 5 ms between cycles to allow for relaxation.

4.2.1 Broadening

The width of spectral lines can be subject to several different broadening mechanisms for example lifetime broadening, Doppler broadening, pressure broadening, spin exchange and power broadening. Here we deal with a solid at cryogenic temperature so Doppler broadening is not applicable, however random local strain fields in solids can have a similar effect on the inhomogeneous profile as Doppler broadening [24]. The power broadening is particularly relevant here, the line width may increase with the laser intensity, though not necessarily [25]. The possibility of power broadening must still be entertained since ion collection will be done with many or high-intensity pulses. When exciting and subsequently letting the ions relax, broadening cannot be avoided therefore the structure that is burned back will not be a perfect rectangular bar but rather a more rounded flattened feature. This must then be made sharper by burning next to the structure afterwards. To account for this, the structure is burnt back a bit wider then the final width such that there will be no rounding of the edges of the structure. Instantaneous spectral broadening is a result of ion-ion interactions [26] and occurs when moving ions from the ground state to the excited state. There will be a change in the permanent static dipole moment, this means that the other ions will experience a different field which means that they experience a frequency shift, which means that it might be a good idea to wait with the next burning pulse until the ions have relaxed to the new state. Excitation-induced optical frequency shifts cause a type of optical dephasing and also broaden the homogeneous line [27].

4.3 Inversion of structure

The collected structure contains three different transitions however, simulating the full six level is too computationally demanding therefore the approximation had to be made that one can take average oscillator strength with respect to the proportions of the collected ions. The average relative oscillator strength for the three transitions would be 0.76 and hence a combination was made between the strongest and weakest of the three transitions to reflect this. The ratio was estimated from the αL ratios in figure 9 to be 4/7 of $|5/2g\rangle \rightarrow |1/2e\rangle$ and 3/7 $|3/2g\rangle \rightarrow |3/2e\rangle$. Other parameters are the maximal Rabi frequency, which was according to calculations 372 kHz and then with the relative oscillator strength taken into account 283 kHz but to have a safety margin was assumed to be 250 kHz. With the sechscan one can in theory pump infinite power into the crystal by scanning infinitely slow. The lifetime of the inversion limits the useful

duration of the sechscan however. T_1 is 2 ms, but with the calculations made for the ASE would be reduced to 1 ms. To remain within acceptable levels of decay one would like to have full inversion the shortest possible inversion pulse. According to simulation the shortest possible inversion pulse for good inversion is 130 μs, the resulting inversion is shown in figure 10.

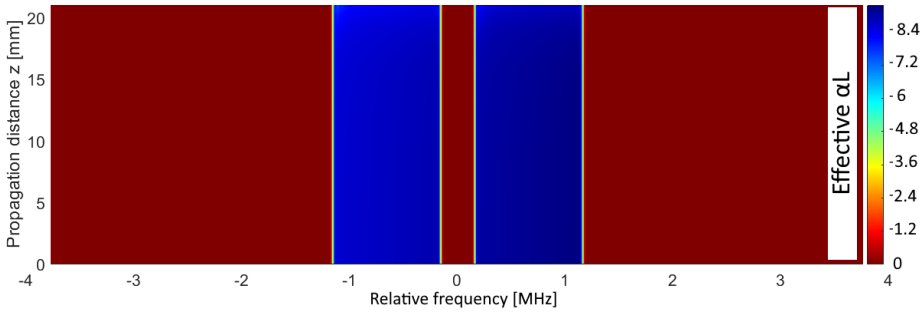

Figure 10: Structure after inversion with a 130 μs sechscan pulse with a scan range of 5 MHz assuming $\Omega = 250$ kHz, The legend is in normalised αL with a transfer efficiency of the strongest transition of 85%, the negative values indicate gain showing that full inversion was achieved through the entire length of the crystal

With this result for the inversion time, the fast light can be optimised. One would like to have the smallest time-bandwidth product pulse. With the simulated structure, the propagation pulse needed to fit within the 300 kHz wide hole in the middle. This was possible with a Gaussian pulse with a cut-off duration of $t_{\text{cut-off}} = 75$ μs and a FWHM in Rabi frequency of $t_{\text{FWHM},\Omega} = 15$ μs. These pulse lengths were needed to make sure the pulse shape was smooth enough and went to zero in the wings sufficiently to not get clipped by the gain structure. Since the desired αL was 12 any power outside the hole would be amplified 163.000 times. The result is shown in figure 11, where the first is given in Rabi frequency and the second in intensity, since power is what will be seen on the detector during the experiment.

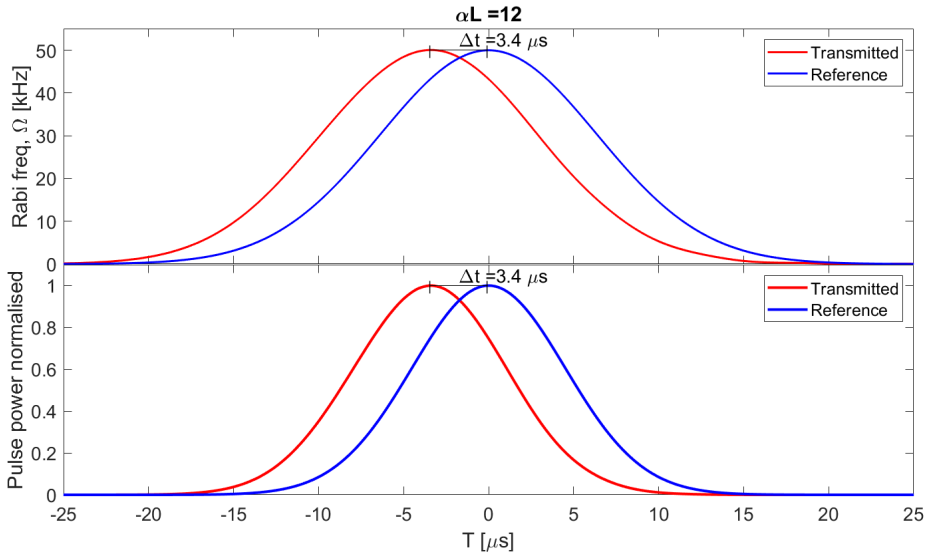

Figure 11: Propagation pulse sent through the designed structure in Rabi frequency and in Power.

From this simulation it is expected that there will be an advancement Δt on the propagation pulse of 3.4 μs, i.e. 23% of the pulse t_{FWHM}.

5 Methodology

5.1 Experimental considerations

We will be dealing with inverted structures. That means that there will be fluorescence to other transitions. Therefore a 580 nm narrow band filter was inserted before the detector. There will be high power on the photodiodes during the transfer of the structure to the excited state. To speed up the recovery times the photodiodes are biased with 9.5 V. In figure 12 the full setup is depicted. The lenses marked by 3, 4 and 8 were standard lenses that were available so the beam reaching lens 8 was not perfectly collimated at the desired beam size but rather slightly converging already. Therefore the focus was checked with a beam profiler. The broadening of the homogeneous linewidth scales with $\Delta\Gamma_h(T) = 0.0018 \cdot T^7$ Hz, [21] The temperature was measured throughout the experiment and ranged between 2.5 K and 4 K depending on the experiment, meaning that at any time the broadening of the homogeneous linewidth was in the hundreds of Hz, which is sufficiently narrow for our application. Due to the extremely long hole-lifetimes [21] once a structure is created, it will not disappear for the duration of the experiment however if needed the laser can be swept over 10-20 GHz repeatedly to re-shuffle the ions. The laser locking cavity has a free spectral range of 3.3 GHz allowing us to move to different positions on the inhomogeneous profile. The transimpedence amplifiers have a gain up to 10^7. At this gain the bandwidth is 220 kHz, the rise time can then be approximated by 0.35/bandwidth, or 1.5 μs at the 10^6 setting they have a bandwidth of 1.2 MHz or a rise time of 0.2 μs. The Frequency of the laser is frequency shifted with a 200 $\pm$ 50 MHz double pass AOM which determines the range for ion gathering. The pulses will be generated with an Arbitrary waveform generator (AWG). For the fast light effect, it is very important that the function is analytical so it must be smooth experimentally or the signal will show high frequency oscillations, hence a new AWG with 14 bits was used to get the needed resolution. Finally a brief note on the pulse shape, several options were considered including a rectangular pulse in frequency (i.e. a sinc in time) and a so-called "Nuttall windowed" pulse but in the end a simple transform-limited Gaussian was chosen because of its time/frequency relation and simplicity.

5.2 Experimental setup

The experiment was conducted with a scannable, narrow line width tuneable CR-699-21 dye laser (Rhodamine 6G) with a λ range of 570-635 nm [22] which is frequency locked using Pound-Drever-Hall locking [28]. The crystal was placed in a Mycryofirm 1.5 K closed cycle cryostat.

5.2.1 Description of the setup

Figure 12 shows the optics used in the experiment and the components are described in table 4.

Table 4: Description of optical components in figure 12

1	PM-fibre	11	Collimating lens
2	Beam pick-off	9	Cryostat
5,12,21	Mirrors	10	Crystal
3,4	Telescoping lenses	14,20	AOMs
6	Halfwave plate	17	Narrowband filter 580 nm
7,16	Polarisers	18,23	Photodiodes
8,13,15,19,22	Focusing lenses	24, 25	Transimpedance amplifiers

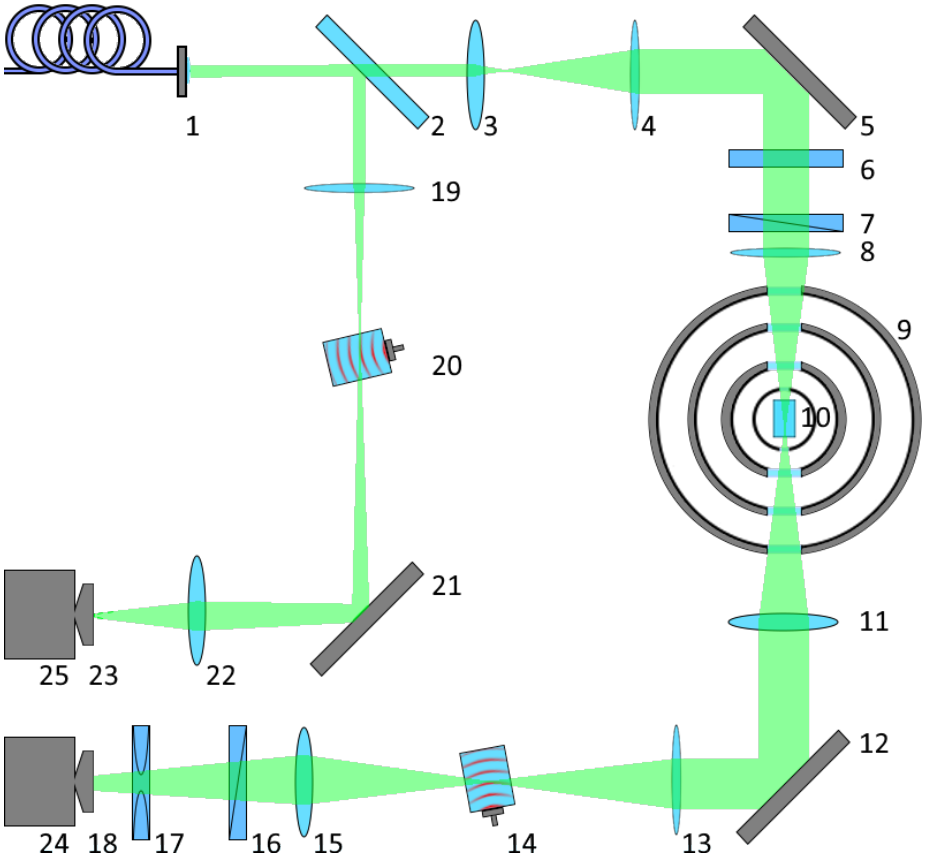

Figure 12: Schematic representation of experimental setup

The light is brought onto the table using a polarisation-maintaining fibre, and a beam pick-off is used to split of part of the beam, that gets sent through an AOM and is then focused on the reference detector. The AOM is needed because there will be a very strong pulse for the inversion followed by a rather weak one for the probe, which does not leave the detector enough time to recover hence

the AOM is used to send the first order to the detector only once the probe pulse is sent, the same applies to the AOM after the cryostat. In the main light path the beam is first expanded, then the polarisation is matched to that of the D1 absorption axis of the crystal with the half wave plate and cleaned up with the polariser and is focused down to 65.6 μm in the middle of the crystal. Only the probe pulse is gated to the transmission detector, but before that it is first cleaned up with another polariser and bandpass filter to remove any fluorescence and any light with different polarisation.

5.3 Experimental procedure

5.3.1 Burning the pit

The burning of the pit is a simple procedure, a frequency sweep is conducted starting at -14.5 MHz to +14.5 MHz from the transition. The frequency range is swept over 1 ms with full power, this is repeated 60 times after which it is read out by another frequency sweep over a range of 50 MHz at low power, (0.1% of full power), and with a duration of 0.5 ms, this is then repeated until we no longer see any improvement in the pit depth, typically 2-3x to be certain. This depth is then assumed to have 0 absorption. The validity of this assumption is discussed in Appendix B2.

5.3.2 Burning back the structure

The burning back of the structure is done with sechscan pulses, with cut-off duration 450 μs, the frequency width of the sechyp is 0.07 MHz, the ramps have a t_{FWHM} of 15 μs, the scan is 1.4 MHz, full power was used wide and 60 repeats. The shape of this pulse can be seen in the appendix in figure 28. The full set of frequencies is split into two for the left (lower frequency) and right peak (higher frequencies), the set for the left peak is burnt first because one of the classes of ions targeted there drops an undesirable ion group at the location of the right peak, which is burnt away before the right peak is burnt back. One set is burnt once, then there is a wait of 4 ms to allow for decay, transitions are not driven down, then repeated. Once the two peaks are in place, the hole and the edges are sharpened with a sechscan each, the parameters of this sechscan were: cut-off duration 290 μs, $t_{\mathrm{FWHM}} = 12$ μs, amplitude 0.1778 of full power. The structure is then probed by sending a Gaussian pulse in through the hole. If the structure is as planned, i.e. $\alpha L = 12$, gain peak widths = 1 MHz, hole width $\Gamma_h = 300$ kHz it is expected to yield a slowlight effect on the order of 3 μs without distorting the pulse. The structure is also read out with a frequency scan at low power and slow scan speed, but this is not done each time as even at little power the ions will be burnt away.

6 Results and Discussion

6.1 Structure characterisation

During the experiments it was observed that the polarisation direction on the table was varying with time, and given that there was a polariser before the crystal and not before the reference detector these fluctuations cannot be compensated for using the reference detector. One can see this in figures 13 and 24 of the readout of the spectral hole at low absorption and a readout over the entire bandwidth of the AOM used to modulate the laser. The absorption is expected to be very low in the hole and for the calculation of the αL it is assumed to be zero at the centre of the pit. This means that due to polarisation fluctuations an artefact can arise that the absorption goes slightly negative. Furthermore, it was noted earlier on in preliminary experiments that one needs only a little power to shuffle away ions and these cannot always be retrieved, which was also seen as consecutive experiments even with re-burning of the structure showed a deterioration of the results, i.e. less fast light and slow light effect after more cycles. The deterioration of the structure can be seen in the appendix in figure 25. Therefore to ensure the best possible results, the experiment was carried out in full; burning the pit and the structure, sending in the initial probe pulse, performing the inversion and then the remaining two probe pulses, before reading out the structures and the empty pit. Because the lifetime of the undisturbed structures is so long, the holes in the inhomogeneous profile resulting from gathering ions remain visible in the readout.

6.1.1 Burning the pit

A pit of width 29 MHz was created, the readout of which is shown in figure 13. Here the approximate absorption coefficient as a function of frequency is shown. As one can see the noise in the high absorption areas is rather high. This is because the transmitted light at these frequencies has such low intensity that it is in the noise limit. Because of said low intensity an exact number for the absorption coefficient cannot be computed this way. However one gets a good impression of the width of the pit. This readout was done by sweeping the frequency over a range of 50 MHz in 0.5 ms at constant amplitude. Towards the lower frequencies of the pit, one can see a hole that resulted from the burn back process of an earlier run.

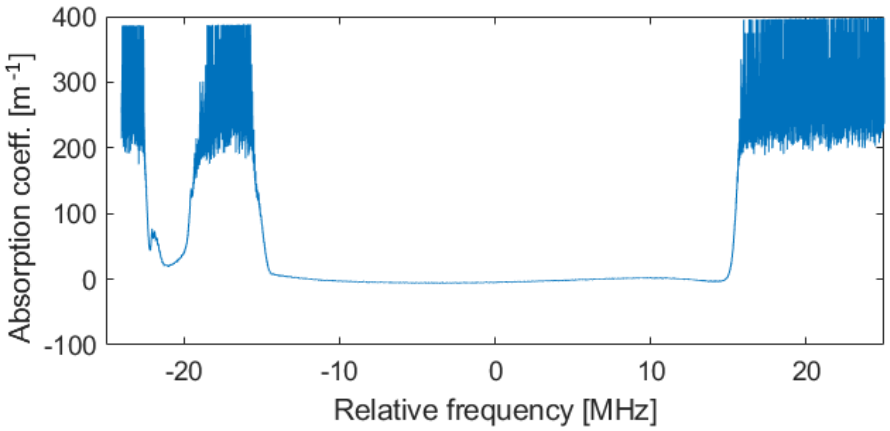

Figure 13: Empty pit created for the structure to be burnt back into, the frequency axis is shifted such that the zero-point lies in the middle of the pit.

The assumption of very low absorption in the middle of the pit is used here to compute the absorption coefficient α, by using this measurement as maximal transmission and then using the reference and the Lambert-Beer law.
The empty pit was used to probe the hyperfine broadening. A narrow Gaussian at frequency detuning of -46.175 MHz of the centre frequency was used to burn back ions into the centre of the pit. This is depicted in figure 14 and 15. This corresponds to probing the broadening of the $|3/2e\rangle$ and $|5/2g\rangle$ levels. The SNR on this readout is not great and polarisation issues are still present which seem to cause some artefacts but with some filtering, it is visible that the full width half maximum of the broadening is about $f_{\mathrm{FWHM}} = 308$ kHz.

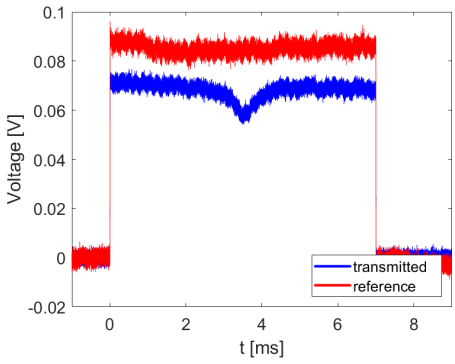

Figure 14: Raw data of readout of hyperfine broadening check

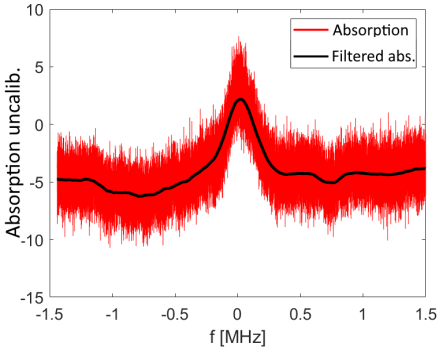

Figure 15: Absorption computed arbitrary units and filtered using a moving mean filter.

6.1.2 Creating the structure

The absorption structure was burnt back into the pit with the sechscan pulses and read out using a constant amplitude frequency scan over 5 MHz with a duration of 7 ms. This gives a resolution of $\frac{\sqrt{\text{Scan-rate}}}{2\pi} = 4.2$ kHz on the width. This readout is seen in figure 16.

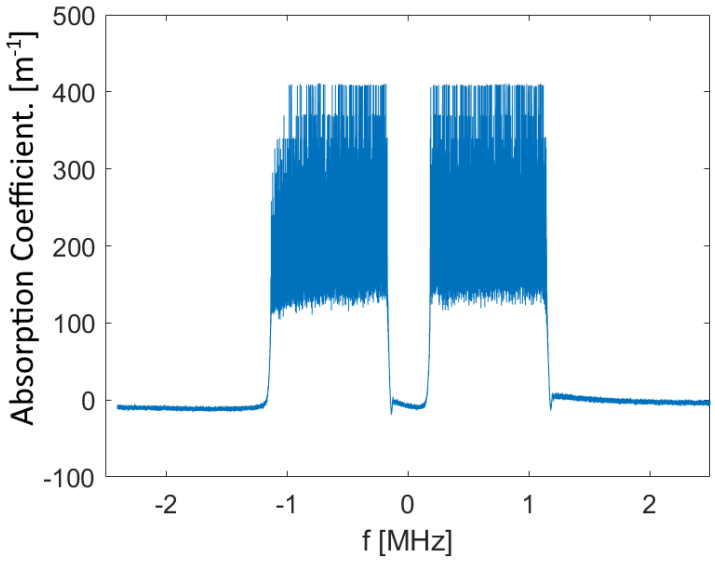

Figure 16: High-resolution readout of the structure created in the middle of the pit. The structure was read out at a scan speed of 2 kHzs^{-1}

A probe pulse (Gaussian) is then sent into the structure to gauge the slowlight effect. When combining this to with the frequency width found from the scan a good estimate can be made of the collected absorption αL. The probe pulse for the slow light effect is depicted in figure 17 B, and is matched with a simulation to extract the αL in figure 17 A. Here one can see very good correspondence between the simulated and experimental pulses both in shape and in pulse delay, this suggests that the structure is indeed clean and symmetrical, and the αL obtained of the structure at the peak of the inhomogeneous profile was 10.5 thus the absorption coefficient $\alpha_{\text{collected}} = 500\ \text{m}^{-1}$

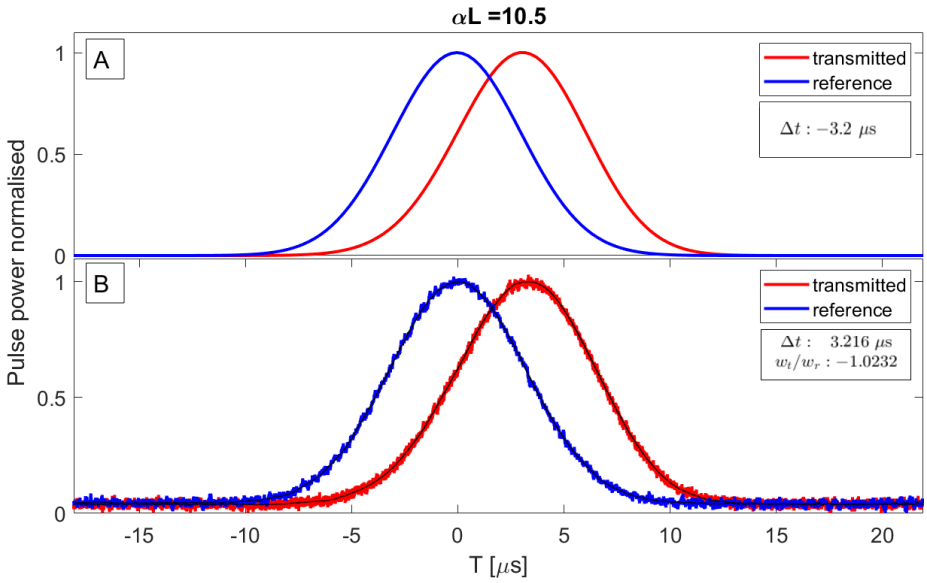

Figure 17: A, Simulated results of a pulse that was sent through the structure with the same width (in frequency) as created in the experiment. Using αL as the variable to determine the absorption of the structure. B, Probe pulse sent through the created absorption structure to estimate αL, the translucent line is the measured data, the solid line within is the Gaussian fit, w_t/w_r is the width ratio of the transmitted to the reference pulse. The experimental pulses are normalised

6.2 Inversion

During the experiment the inversion did not perform nearly as well as it did in simulation. Which suggests that the Rabi frequency was much lower than anticipated. When examining the power at various stages in the light path it was found that the polarisation out of the fibre was rotating in time and the power after the optics on the table was lower than expected as well. An attempt was made to resolve this but this was not fully achieved. The power in

front of the cryostat was 20 mW, giving $\Omega \approx 245$ kHz, which should have been enough according to the safety margin in the simulations, where we worked with $\Omega = 250$ kHz. After disassembling the cryostat it was also noticed that during the last part of the experimental run, the beam had likely been clipping the side of the cryostat window. Near the edge of the window, there is a glue layer that may have been scattering, absorbing and reducing the beam quality. The expected Rabi frequency was around 360 kHz, assuming we would have 30 mW at the cryostat, the real value was thus much lower. Hence the experiment would not work as well as designed.
In an effort to get sufficient power to the crystal, the inversion pulse duration was increased to last 720 μs instead of the 130 μs that was determined to be optimal according to simulations. The αL of 10.5 was also too high therefore had to be readjusted as well to avoid getting a slow-light effect due to insufficient inversion. So the pit and structure were moved from the peak of the inhomogeneous line to lower absorption.

6.3 Fast and slow light results

Using the slow-light effect as an indicator the αL at this frequency was 4.8. The probe pulse was then reduced in t_{FWHM} to 5 μs as at this gain the experiment is less sensitive to power into the structure. The probe pulses were sent in using the following sequence: one slow light probe pulse, 15 ms wait, one inversion pulse immediately followed by a probe pulse, 15 ms wait and finally another slow light pulse. This pulse sequence is shown in figure 18 It was observed that there was some amplification after the inversion on the fast light probe and some attenuation on the slow light probes (see also figure 26).

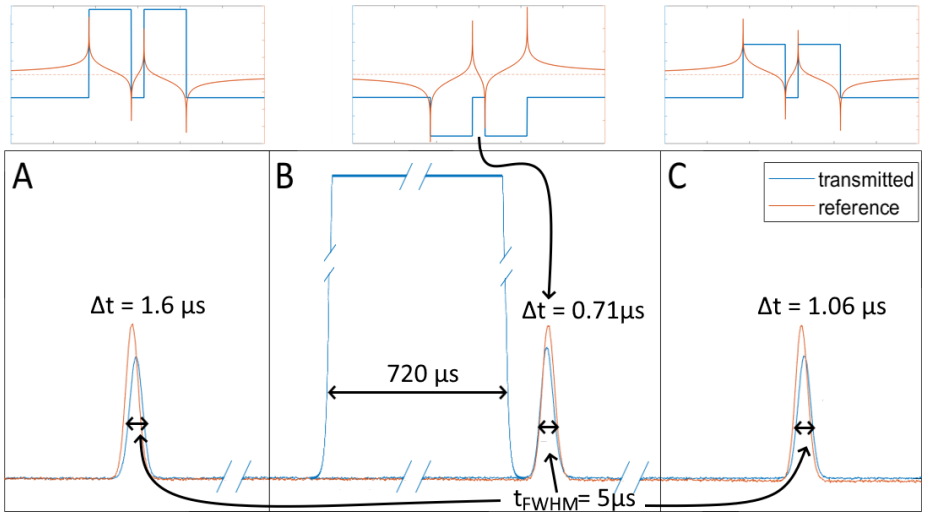

Figure 18: Pulse sequence with inversion pulse spliced in, not to scale compared to the probe pulses. Line breaks indicate skipping forward in time to fit the graphs in the figure.

Simulations showed attenuation of the peak in all three cases and in the plot for the Rabi frequency (figure 27 in the appendix). During further simulations, it was found that this is likely related to the pulse intensity. It was possible, by increasing the Rabi frequency, to get a slight amplification on the transmitted pulse compared to the reference. This also negatively affected the t_{adv}. It was seen that there is some minor ringing in the simulations for the Rabi frequency. Since the measured data is in power and hence the square of the Rabi frequency this is much harder to see. It can be seen in the experimental data where it deviates from the fit, so it is thought that the probe pulse clips the structure slightly. At this duration of the inversion pulse the decoherence and decay become significant factors therefore at the time that the probe pulse is sent in the upper state population will have reduced. The upside is that with less inverted population, lower absorption and hence lower αL the effect of ASE will also be much lower. With these parameters, a significant advancement with respect to the pulse t_{FWHM} was achieved, see figures 19 and 20. The pulse advancement was 0.71 μs which is 14.2 % of the t_{FWHM} using this the group refractive index is then calculated to be n_g =-10135.

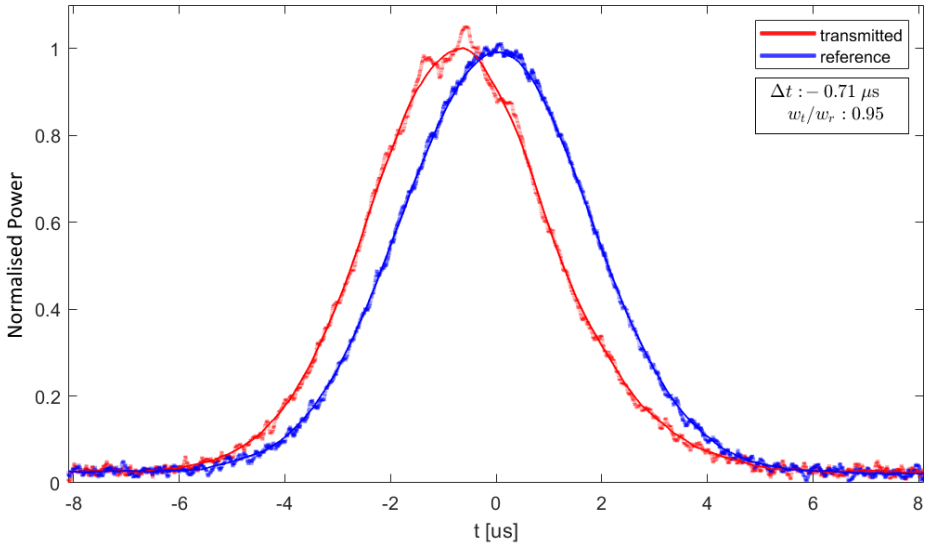

Figure 19: Experimental fast light data normalised. Both filtered and unfiltered are presented. The former with the slightly translucent line and the latter the solid line.

There is some structure on both the fast light and slow light pulses presented here. This was not present on all experimental fast light pulses (see figure 30), crucially those that seem to have this behaviour had higher amplitudes on the probe pulses. After further investigation is thought to be a non-linear effect of too high amplitude, which is why it is present on all three pulses, this behaviour was also observed in simulations. Furthermore, in the two works by Wang, Kuzmich and Dogariu [2], [12], this can also be seen, in their first publication there is some periodic structure on the transmitted pulse whereas in their second publication the transmitted pulse is perfectly smooth, seemingly the difference between the two situations being a reduction in pulse amplitude by a factor ten. The filtered and normalised three pulses with their simulations to match are presented in figure 20 B and A respectively

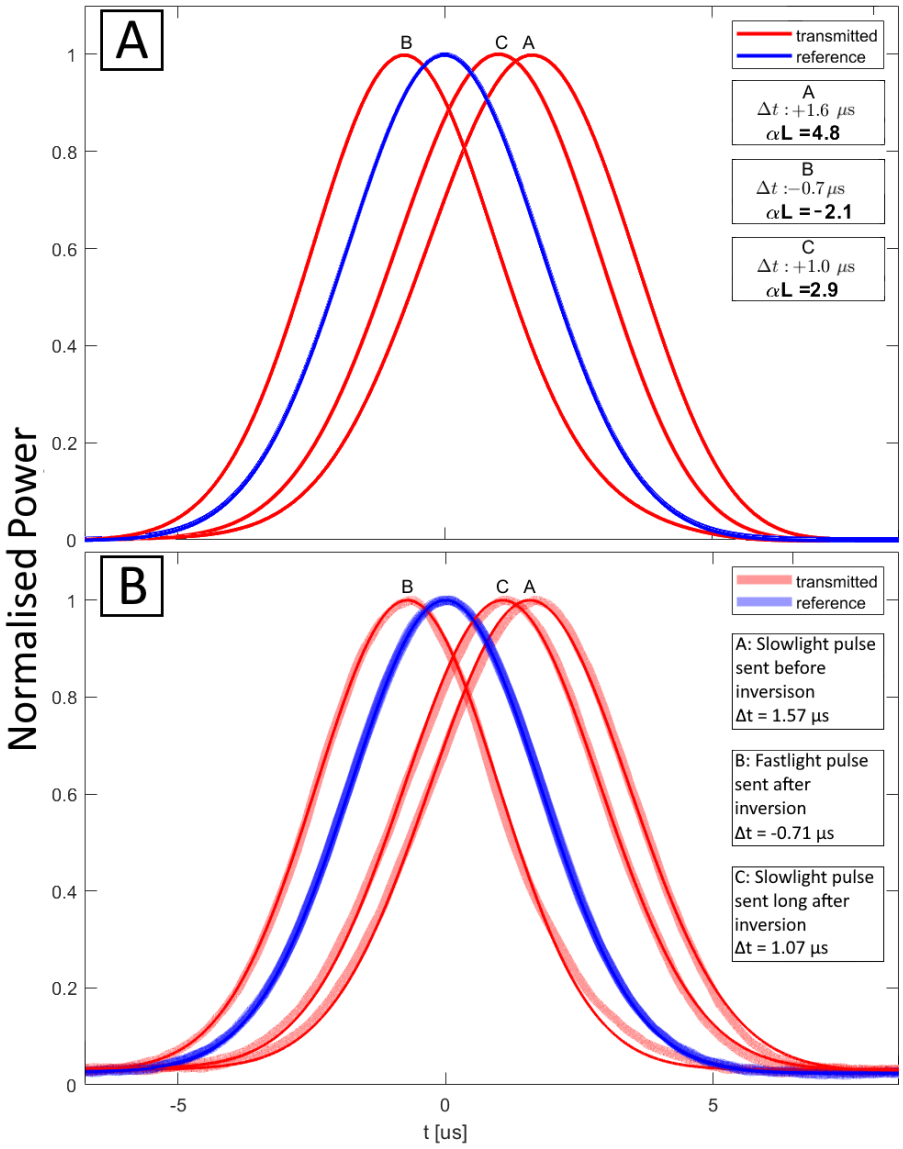

Figure 20: Fast light and slow light pulses simulated to match experimental data (A) and experimental data (B). Fitted data is presented in solid lines, experimental data in translucent lines. Here is is a bit more easy to see the slight tail that likely resulted from slightly clipping the structure.

Then the slow light before the inversion is plotted against the slow light long after the inversion in figure 21 for several runs. It shows a very clear linear relation that corresponds quite closely to the average oscillator strength for

the three transitions suggesting that letting the exited ions relax causes them to fall down according to their oscillator strengths. This indicates that the relaxation probability to the different hyperfine levels scales roughly with the relative oscillator strengths see table 2. This was outside the scope of this thesis however and has not been thoroughly investigated. If the three gathered transitions per isotope made up equal portions of the gathered αL the average relative oscillator strength would be 0.76 and the ratio of ions returning to the structure from experiment is 0.71.

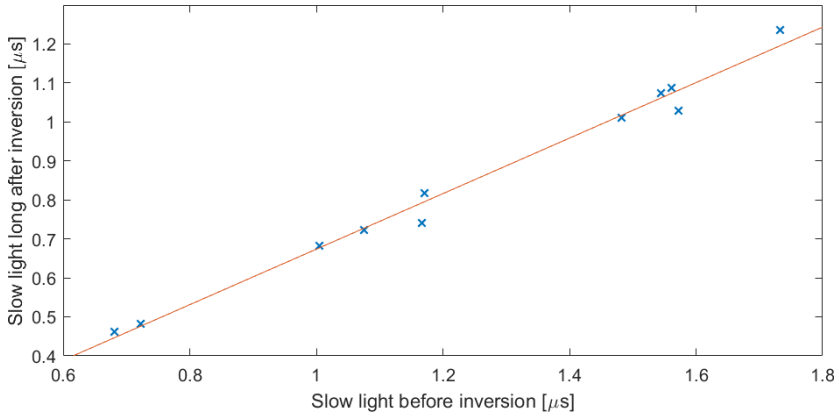

Figure 21: The slow light before inversion is plotted against the slow light long after the inversion, a linear fit was added with a slope of 0.71

The inversion success rate is estimated by the ratio fast light over slow light before inversion, Inversion-degree $= \frac{1}{2} - \frac{t_{\text{adv}}}{2t_{\text{delay}}}$. This can be seen in figure 22.

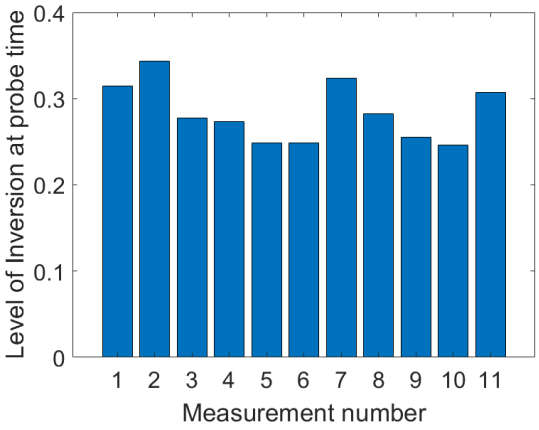

Figure 22: Degree of inversion achieved for several measurements

One of the experimental pulses is plotted as a function of space in figure 23 at different snapshots in time. Where it can be seen that the pulse starts to emerge from the far side of the crystal before fully entering, in the third panel it is visible that the pulse peak has not yet entered the crystal, but has already started to come out at the end. Here for the incoming pulse, the reference data is used and for the advanced pulse the transmitted data, the incoming pulse is then shifted until it 'touches' and disappears into the crystal and the transmitted is shifted and starts to appear as it would come out of the crystal.

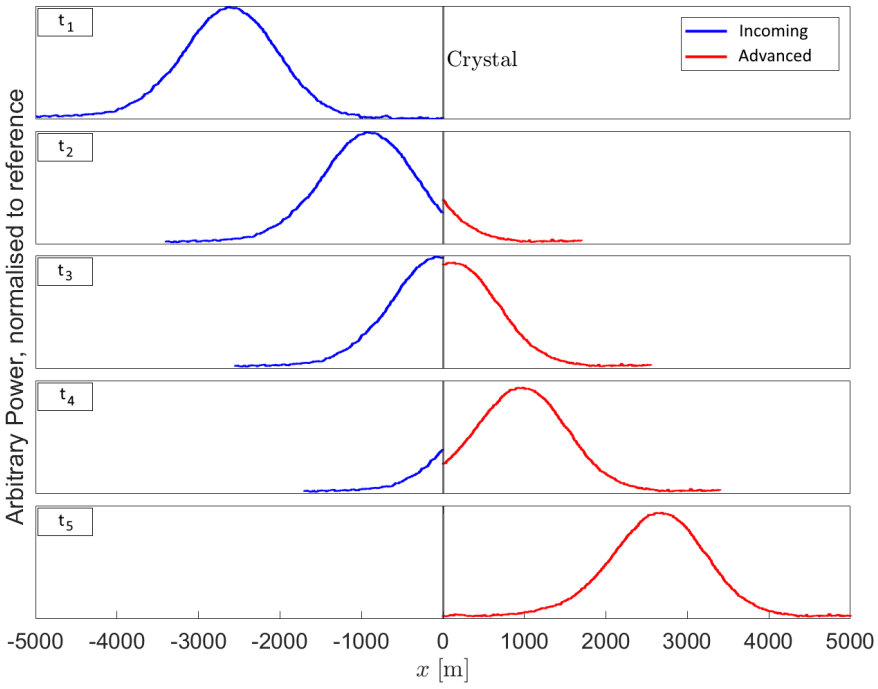

Figure 23: Spatial propagation of an experimental fast light pulse.

6.4 Issues with laser power at the crystal

A readout was taken over the full frequency range of the AOM in between the re-burning of the structure, this is shown in figure 24.
Firstly it is a nice overview of all the ranges in frequency where ions were burnt away from and that even after the structure is removed from the centre of the pit, there are ions that are not returned to their original state. This shows again some ions can only be collected once and more are lost with each cycle. It also shows the fluctuation in the power of the laser over time, the difference between the degree of fluctuations between the reference and the transmitted is an indication that the polarisation may change with time. The residual rotation

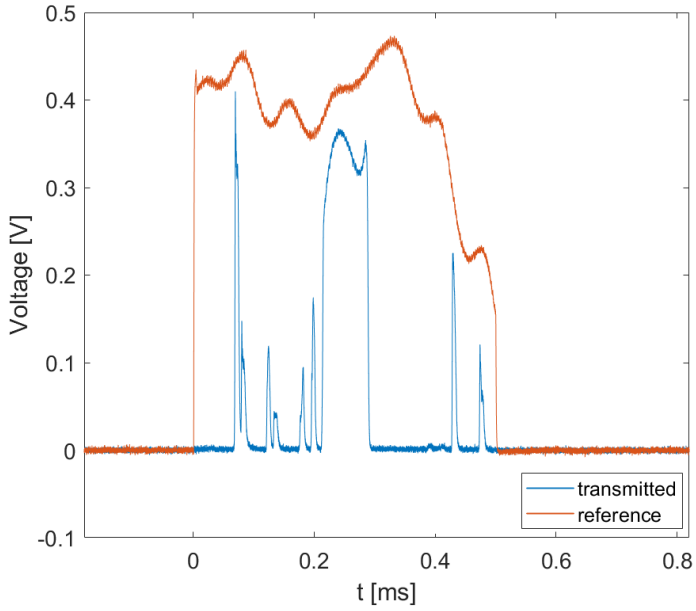

Figure 24: Readout of the full structure with reference signal included

of the polarisation likely occurs in the fibre which acts as a very high order $\lambda/2$ plate when it is not coupled in correctly. It is expected that the laser power is frequency dependent as the AOM efficiency is not constant in frequency, but not to this degree.

7 Conclusion and Outlook

7.1 Conclusion

To conclude, in this thesis a recipe was created for generating negative group velocity in a rare-earth-ion-doped crystal. The precise creation of a spectral pit with an absorbing structure was simulated and optimised. The dispersion of the refractive index was theoretically derived and plotted. Maxwell-Bloch simulations using software developed by Adam Kinos [23] showed it should be possible create and subsequently invert a structure with an αL of 14 and giving negative dispersion between the peaks to achieve a pulse advancement of about 30% in the optimal case in Eu:YSO. Pulses for all steps were programmed and successfully tested. Experiments showed that an αL of 10.5 can be collected, possibly more if the AOM range is extended. A stumbling block was the laser power reaching the crystal, which was not near sufficient for the intended inversion step. The beam quality was most likely ruined due to improper alignment with the cryostat window massively reducing the power. By adapting the pulse length of the inversion pulse and the probe pulse and moving further to the side

of the inhomogeneous profile it was possible to demonstrate a pulse advancement of 14% of the t_{FWHM} with minimal pulse distortion or absorption and a n_g of ≥ 10000 achieved this is to my current knowledge the largest relative pulse advance achieved in this configuration to date without any significant pulse distortion. The literature search on this has not yet been absolutely exhaustive however.

7.2 Outlook

There are a few very straightforward changes that could be made to improve on the experiment, firstly stabilising the polarisation coming out of the PM fibre to the table should be addressed, some is lost in this step already. More extensive calibration for the duty-cycle of the AOM tailored to this specific pulse sequence might allow for better coupling into the fibre. The gating AOM's were added late in the run so optimising their alignment might give an improvement in signal on the detectors. And finally we believe the most important factor to improve is the alignment through the crystal, it might actually be wise to do this before fully assembling the cryostat as the four windows give many reflections and the gold coated thermal shields and mirrors on the crystal aggravate this effect making it difficult to see what is actually being hit. With all this in place the power delivered to the crystal should be much higher and one could consider making the gain structure wider to increase the effect. Furthermore it might be wise to increase the pulse duration and decrease the hole width such that the bandwidth of the detectors is less limiting. As a matter of fact higher gain and more bandwidth would be good too. And finally having access to the RF erasure would allow for a quick reset and allowing for a proper return to zero after a number of experiments.

8 Acknowledgement

First of all I would like to thank the Quantum information group as a whole for the great study environment, hygge and everyone's willingness to always contribute with discussions and insights. Thanks to Abdullah for telling me I actually had to turn on the AWG for it to work. David Hill for help with a temperamental laser. Then thanks to the people more directly involved in several discussions on the experimental execution, goals, and discussions / explanations of theory: Stefan Kröll, Andreas Walter. And a special thanks to Lars Rippe, Adam Kinos, David Gustavsson for being my main supervisors, and for, together with Marcus Lindén, answering seemingly infinite questions from me, always being happy to help with simulations and experimental problems spending several late nights in the lab to get things right.

Thanks Robert, Andrea and Saga for all the good times it's been a blast.
And last but not least, Alena, Anna, Gonda, Jeska, Leon and Miriam thanks for all the support.

Appendices

A Thermal distribution

In the canonical ensemble, fixed temperature volume and number of states the probability distribution to find an ion in a given state s is given by [29]:

$$P_s = \frac{1}{Z} e^{-\beta E_s} \tag{60}$$

with $\beta = 1/(k_b T)$ and Z the partition function.

$$Z = \sum_s e^{-\beta E_s}$$

so the probability ratio between to states is:

$$\frac{P_s}{P_m} = e^{\beta \Delta E_{sm}} \tag{61}$$

B Supplementary Data

B.1 Deteriorated structure

As mentioned it was noted that the structure deteriorates after some inversion cycles, a quick readout of this was taken after the experiment was finished. This readout is depicted in figure 25 which shows that the αL was significantly reduced and the sharp shape of the structure has also been lost. They are now more triangular than rectangular, which is sub-optimal. The resolution on this readout isn't as high but from the propagation pulses it also seems that it is broadened and some ions fall into the hole.

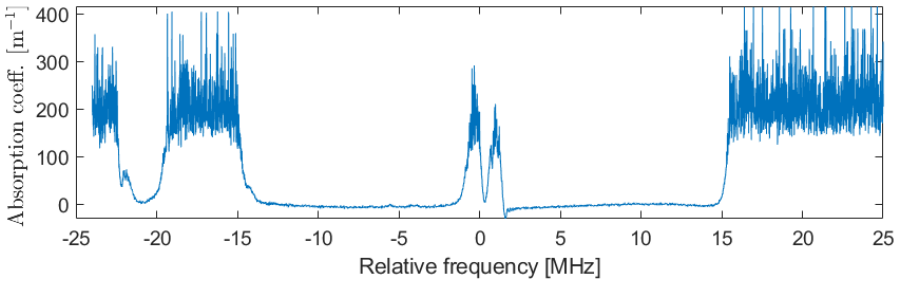

Figure 25: Readout of the structure after inversion and probing, quick readout of 0.5 ms over 50 MHz range.

B.2 Structure clipping

The reason I feel there is a strong case that the probe pulse is clipping the structure is that if one looks at the power of the three pulses in figure 26 the inverted is slightly amplified as compared to the other two and has a tiny bit of a tail trailing the pulse. The slow light pulses here also are minorly misshapen in the same way.

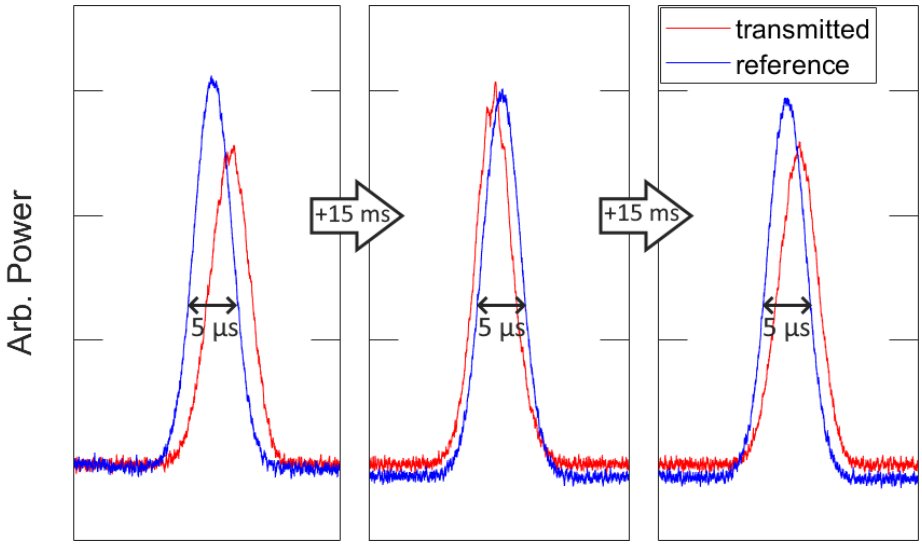

Figure 26: Three identical Gaussians sent through the created structure subsequently, unfiltered raw data. Left pulse is long sent in before any inversion. The middle pulse is sent in right after inversion. The right pulse is sent in 15ms after inversion.

In a simulation to mimic the experimental conditions, where the pulse is made narrower in time, the structure is kept the same width but the αL is reduced, we can see the same thing as was shown in the results section. The probe pulses have a bit of a tail trailing them. Moreover, when looking at the Rabi frequencies of these pulses the origin of the tails becomes apparent, it is the very low amplitude ringing due to clipping the structure. And in these simulations, the main peak amplitude attenuation for the fast and slow light cases respectively is seen in figure 27 A and B. However in the actual experiment the amplitude ratio of the fast light pulse over the reference pulse is noticeably higher than that of the slow light pulses over their respective reference pulses. This indicates that some small amount of absorption is still present in the pit.

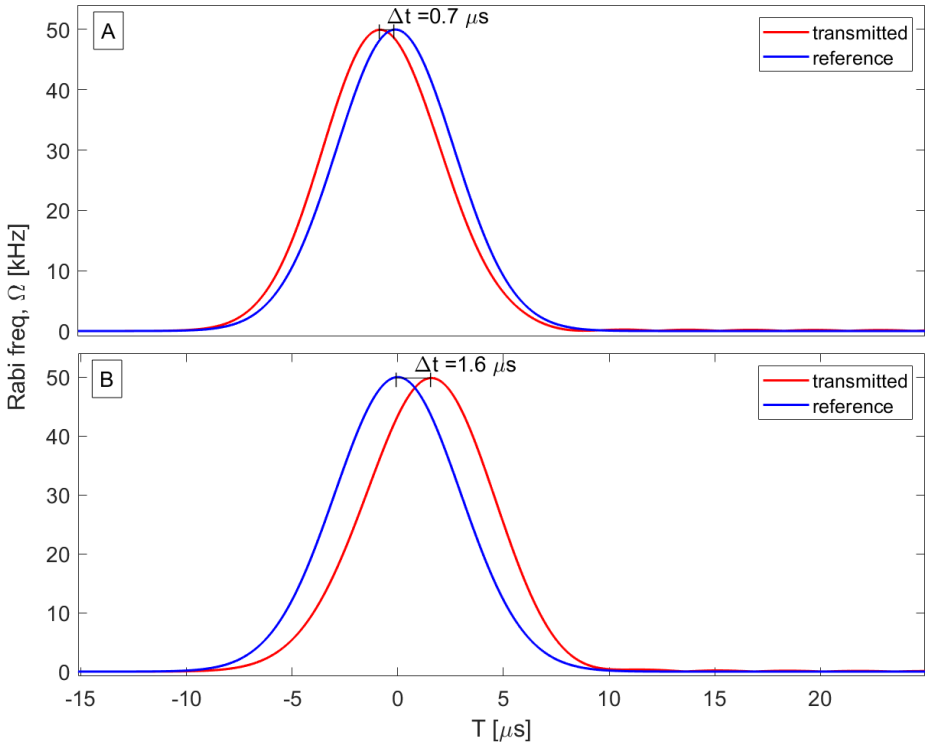

Figure 27: Simulations made to match experimental pulses. A) Fastlight simulation with effective αL 2.1. B) Slowlight simulation with effective αL 4.8.

B.3 Pulse shapes used in experiment

This section serves to give descriptions of some of the pulses used and to reflect on some of the results that may not be the most interesting for the scope of the thesis.

B.3.1 Inversion pulse

To deal with the substantial power deficiency, the back-burn pulses were also altered to be longer, this was done during the experimental run so the cut-off duration was not optimised as can be seen in figure 28

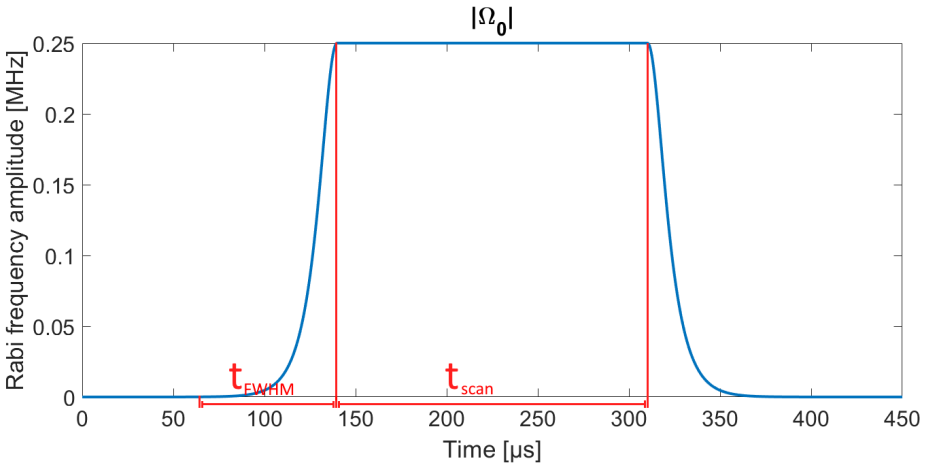

Figure 28: Sechscan pulse used for the collection of ions for the gain peaks, indicated are the t_{FWHM} of the sechyp and the $t_{scan} = \frac{f_{scan}}{Scanrate}$

B.3.2 Unfiltered non-normalised propagation pulses: slowlight

The initial slowlight probe is depicted in figure 29. The data depicted in this plot was done with a slightly different setup than the later data sets. To probe the structure no inversion pulse was needed and hence at this time during the experiment, there were no AOMs used to gate the probe pulse. It was initially expected that the recovery time of the detectors would be sufficiently quick that no gating was needed which turned out to be incorrect. This meant that the optical path was elongated, more elements were introduced and the focus in the crystal was re-aligned. The window-clipping issue likely arose during this process. As one can see the transmitted pulse in the earlier data is stronger than the reference pulse but if one then looks at figure 26 for example it is weaker than the reference.

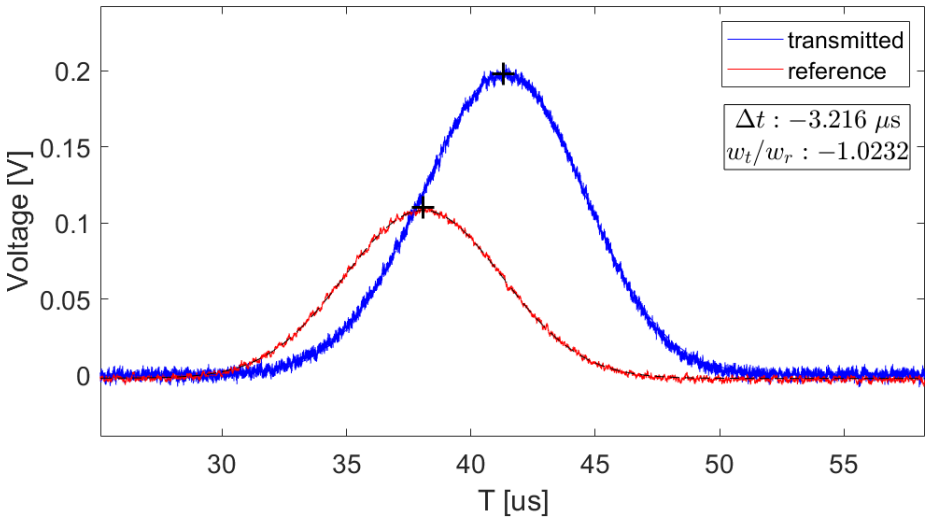

Figure 29: Unfiltered and un-normalised slow light through structure with $\alpha L = 10.5$

B.3.3 Unfiltered normalised propagation pulses: fastlight

Figure 30 shows a number of the fast light pulses that were recorded during the experimental run. All pulses are normalised but unfiltered. It can be seen in C,F and J that the propagation pulses became a bit jagged. This is presumably related to the amplitude. In B the fast light is close to the amount in C, 0.54 mus compared to 0.71 μs without any distortion present.

Table 5: Pulse advancements in [μs] of pulses in figure 30

A	B	C	D	E	F	G	H	I	J
0.43	0.54	0.71	0.54	0.36	0.55	0.65	0.49	0.35	0.55

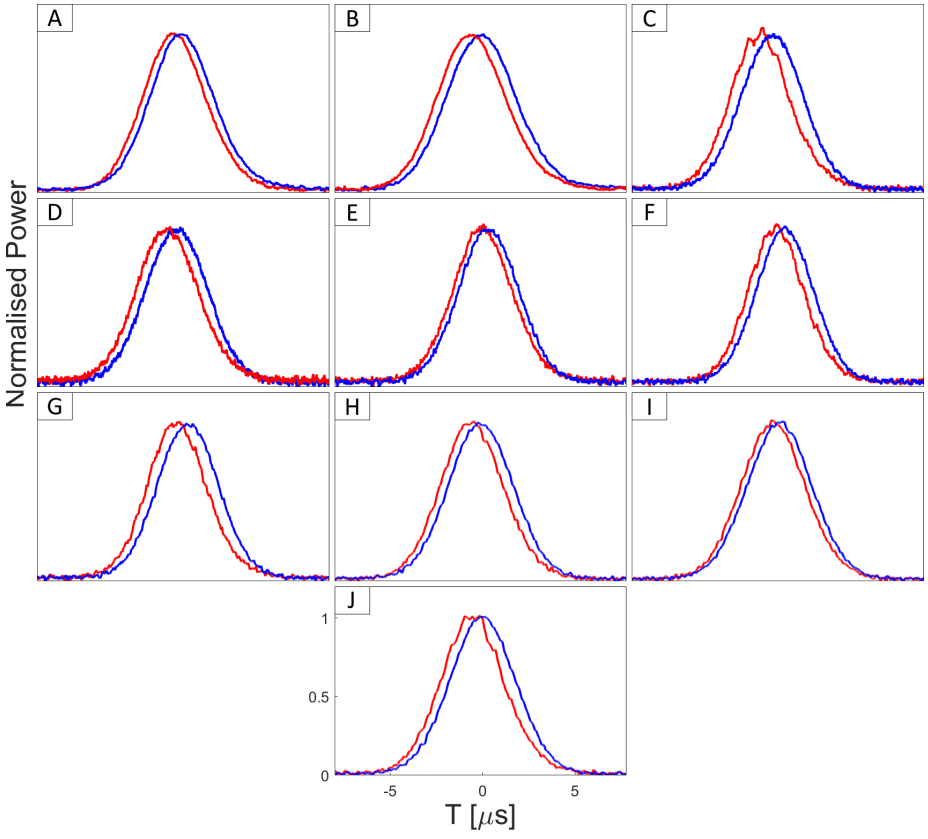

Figure 30: Fast light pulses recorded

B.3.4 Propagation inside the gain structure

Out of curiosity a pulse that was purposely chosen to be far too broad in frequency was sent into the inverted structure. The resulting data is presented in figure 31, where it is seen that there is a peak that is advanced and amplified a lot compared to the reference followed by a ringing tail, which still has a bit of a Gaussian envelope to it. This seems to, partially, present the same behaviour as what Basov et al. [7] have shown for the non-linear amplification case. Here part of the pulse gets extra momentum and part of it lags behind, but since not all of the pulse is within the gain line some of the frequency content is not being amplified or attenuated in the same way. The ringing one can see stems from the amplification of the frequency components that lie within the gain structure and hence get amplified, whereas frequency components within the transparent frequency ranges do not.

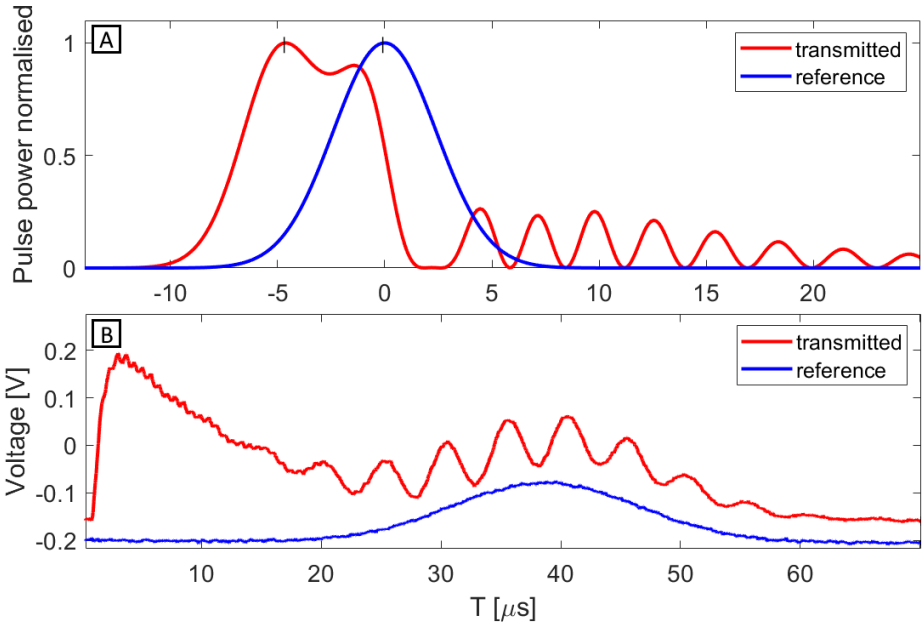

Figure 31: A) Simulation of a pulse too wide in frequency to fit between the two gain lines, B) Experimental data of a pulse too wide to fit between the gain lines. The simulation was not made to match exactly, just to explain the shape seen.

B.4 Back-burning of structure

To simulate the burn-back pulses and to see how to define the parameters such that the edges of the structure are very sharp, Maxwell-Bloch simulations of a two-level material were done. In figure 32 a simulation of a 21 mm long

crystal, with an absorption over a range of 5 MHz (only 3 MHz) that it has been subjected to a sechscan pulse designed to excite a 1 MHz broad region is depicted. As these are the back-burn pulses it isn't vital that the whole length of the crystal is inverted on the first go as there will be several cycles and the absorption at the beginning of the crystal will be reduced with each cycle until it is zero.

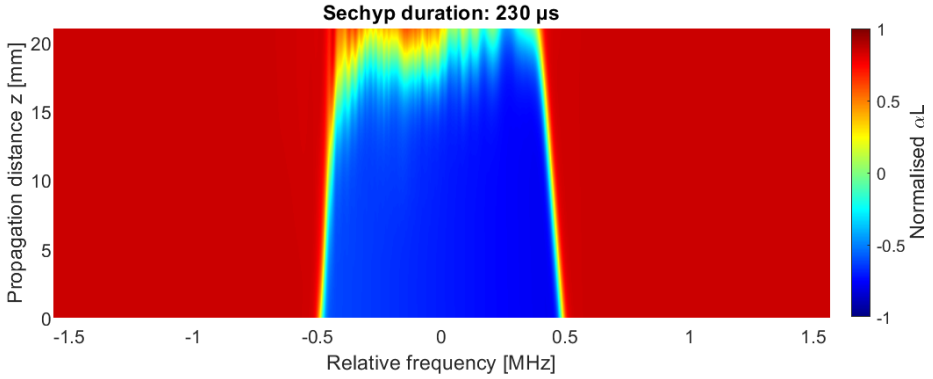

Figure 32: Back burn pulse simulation for a peak of width 1 MHz

Similar simulations are performed for cleaning up the structure. This is done with a 0.3 MHz wide sechscan in for the hole, and 0.5 MHz wide sechscans for the edges as it is not certain how much the broadening will be and absorption outside our gain structure will be close enough in frequency to strongly affect the fast light effect.

References

[1] D.J. Gauthier and R.W. Boyd. Fastlight, slow light and optical precursors: what does it all mean?, Jan 2007.

[2] A.Dogariu, A.Kuzmich, and L.J.Wang. Transparent anomalous dispersion and superluminal light-pulse propagation at a negative group velocity. *Phys. Rev. A*, 63, 2001.

[3] S.Chu and S.Wong. Linear pulse propagation in an absorbing medium. *Physical Review letters*, 48:738–741, 1982.

[4] B.Segard and B.Macke. Observation of negative velocity pulse propagation. *Physics Letters*, 109A:213–216, 1985.

[5] Z.Wang and H.Shen. An electronic circuit principle and test platform for negative group delay and superluminal propagation. *Conference paper, In-*

ternational Conference on Computer Network, Electronics and Atomation ICCNEA, 2022.

[6] R.P.Rajan, A.Redbane, and H.Riesen. Rapid switching between slow and fast light by frequency modulated transient spectral hole-burning. *Journal of the optical society of america B*, 32, 2015.

[7] N.G.Basov, R.V.Ambartsumyan, V.S.Zuev, P.g.Kryukov, and V.s.Letokhov. Nonlinear amplification of light pulses. *Soviet Physics JETP*, 23, 1966.

[8] A.M.Steinberg, P.G.Kwiat, and R.Y.Chiao. Measurement of the single-photon tunneling time. *Phys. Rev. Lett.*, 71, 1993.

[9] D.L.Fisher and T.Tajima. Superluminous laser pulse in an active medium. *Physical Review Letters*, 71, 1993.

[10] R.Y.Chiao. Superluminal (but causal) propagation of wave packets in transparent media with inverted atomic populations. *Phys. Rev. A*, 48, 1993.

[11] A.M.Steinberg and R.Y.Chiao. Dispersionless, highly superluminal propagation in a medium with a gain doublet. *Phys. Rev. A*, 49, 1994.

[12] L.J.Wang, A.Kuzmich, and A.Dogariu. Gain-assisted superluminal light propagation. *Nature*, 406:277–279, 2000.

[13] C.J. Foot. *Atomic Physics*. Oxford university press, 2005.

[14] A.Walter. Cohrent processes in rare-earth-ion-doped solids. *PhD thesis*, pages 12–14, 2009.

[15] R.C. Hilborn. Einstein coefficients, cross sections, f values dipole moments and all that. *Am.J.Phys*, 50:982–986, 1982.

[16] A.E. Siegman. *Lasers*. University Science Books, 1986.

[17] B.E.A. Saleh and M.C. Teich. *Fundamentals of Photonics*. Wiley, 2019.

[18] S.P.Horvarth, C.Shi, D.Gustavsson, A.Walter, A.Kinos, S.Kröll, and L.Rippe. Slow light frequency reference cavities - proof of concept for reducing the frequency sensitivity due to length fluctuations. *New Journal of Physics*, 24, 2021.

[19] C.W.Thiel, T.Böttger, and R.L.Cone. Rare-earth-doped materials for applications in quantum information storage and signal processing. *Joural of Luminescence*, 131:353–361, 2011.

[20] B.Lauritzen, N.Timoney, N.Gisin, M.Afzelius, H. De Riedmatten, Y.Sun, R.M. Macfarlane, and R.L.Cone. Spectroscopic investications of Eu^3+Y_2SiO_5. *Physical Review B*, 85:1–10, 2012.

[21] F.Könz, Y. Sun, C.W.Thiel, R.L.Cone, R.W.Equall, R.L.Hutcheson, and R.M.Macfarlane. "Temperature and concentration dependence of optical dephasing, spectral-hole lifetime, and anisotropic absorption in $Eu^{3+}SiO_5$". *Physical review B*, 68:1–9, 2003.

[22] A.Kinos. Light-Matter Interaction and Quantum Computing in Rare-Earth-Ion-Doped Crystals. *PhD thesis*, pages 89–95, 2018.

[23] Adam Kinos, Lars Rippe, Andreas Walther, and Stefan Kröll. Microscopic treatment of instantaneous spectral diffusion and its effect on quantum gate fidelities in rare-earth-ion-doped crystals. *Phys. Rev. A*, 105:032608, Mar 2022.

[24] L.Allen and J.H.Eberly. *Optical resonance and two-level atoms*. John Wiley and Sons, 1975.

[25] N.V.Vitanov, B.W.Shore, L.Yatsenko, K.Böhmer, T.Halfmann, T.Rickes, and K.Bergmann. Power broadening revisited: theory and experiment. *Optical Communications*, 199:117–126, 2001.

[26] N.Kunkel, A.Ferrier, C.W.Thiel, M.O.Ramirez, L.E.Bausá, R.L.Cone, A.Ikesue, and P.Goldner. Rare-earth doped transparent ceramics for spectral filtering and quantum information processing. *APL materials*, 3, 2015.

[27] J.Huang, J.M.Zhang, A.Lezama, and T.W.Mossberg. Excess dephasing in photon-echo experiment arising from excitation induced electronic level shifts. *Physical review letters*, 63, 1989.

[28] E.D. Black. An introduction to pound-drever-hall laser frequency stabilisation. *American Journal of Physics*, 69, 2001.

[29] H.Gould and J.Tobochnik. *Statistical and Thermal Physics*. Princeton Press, 2010.